

# VOTCA-XTP

## EXCITON TRANSPORT SIMULATIONS

### USER MANUAL



compiled from: 1.5-dev (gitid: f7e5739)

February 16, 2019

[www.votca.org](http://www.votca.org)

## Disclaimer

This manual is not complete. The best way to start using the software is to look at provided tutorials. The reference section is generated automatically from the source code, so please make sure that your software and manual versions match.

## Citations

Development of this software depends on academic research grants. If you are using the package, please cite the following papers

[1] Microscopic simulations of charge transport in disordered organic semiconductors, Victor Rühle, Alexander Lukyanov, Falk May, Manuel Schrader, Thorsten Vehoff, James Kirkpatrick, Björn Baumeier and Denis Andrienko  
*J. Chem. Theor. Comp.* **7**, 3335, 2011

[2] Versatile Object-oriented Toolkit for Coarse-graining Applications  
Victor Rühle, Christoph Junghans, Alexander Lukyanov, Kurt Kremer and Denis Andrienko  
*J. Chem. Theor. Comp.* **5**, 3211, 2009

## Development

The core development is currently taking place at the Max Planck Institute for Polymer Research, Mainz, Germany and TU/e Eindhoven.

## Copyright

VOTCA-XTP is free software. The entire package is available under the Apache License. For details, check the LICENSE file in the source code. The VOTCA-XTP source code is available on our homepage, [www.votca.org](http://www.votca.org).

# Contents

<b>1</b>	<b>Introduction</b>	<b>1</b>
<b>2</b>	<b>Theoretical background</b>	<b>3</b>
2.1	Workflow . . . . .	3
2.2	Material morphology . . . . .	3
2.3	Conjugated segments and rigid fragments . . . . .	4
2.4	Neighbor list . . . . .	6
2.5	Reorganization energy . . . . .	6
2.5.1	Intramolecular reorganization energy . . . . .	6
2.5.2	Outersphere reorganization energy . . . . .	7
2.6	Site energies . . . . .	8
2.6.1	Externally applied electric field . . . . .	8
2.6.2	Internal energy . . . . .	9
2.6.3	Electrostatic interaction energy . . . . .	9
2.6.4	Induction energy - the Thole model . . . . .	10
2.7	Transfer integrals . . . . .	12
2.7.1	Projection of monomer orbitals on dimer orbitals (DIPRO) . . . . .	13
2.7.2	DFT-based transfer integrals using DIPRO . . . . .	14
2.7.3	ZINDO-based transfer integrals using MOO . . . . .	17
2.8	Charge transfer rate . . . . .	17
2.8.1	Classical charge transfer rate . . . . .	17
2.8.2	Semi-classical bimolecular rate . . . . .	18
2.8.3	Semi-classical rate . . . . .	18
2.9	Master equation . . . . .	19
2.9.1	Extrapolation to nondispersive mobilities . . . . .	19
2.10	Stochastic Networks . . . . .	20
2.10.1	Coarse-grained morphology . . . . .	20
2.10.2	Charge transport network . . . . .	23
2.11	Macroscopic observables . . . . .	26
2.11.1	Charge density . . . . .	26
2.11.2	Current . . . . .	27
2.11.3	Mobility and diffusion constant . . . . .	27
2.11.4	Spatial correlations of energetic disorder . . . . .	28
2.12	Random Facts . . . . .	28
2.12.1	xqmm . . . . .	28
2.12.2	EWALD . . . . .	28
2.12.3	GW-BSE . . . . .	29

<b>3</b>	<b>Input and output files</b>	<b>33</b>
3.1	Atomistic topology . . . . .	33
3.2	Mapping file . . . . .	35
3.3	Molecular orbitals . . . . .	36
3.4	Monomer calculations for DFT transfer integrals . . . . .	37
3.5	Pair calculations for DFT transfer integrals . . . . .	39
3.6	DFT transfer integrals . . . . .	41
3.7	State file . . . . .	42
<b>4</b>	<b>Reference</b>	<b>45</b>
4.1	Programs . . . . .	45
4.1.1	xtp_map . . . . .	45
4.1.2	xtp_run . . . . .	45
4.1.3	xtp_tools . . . . .	45
4.1.4	xtp_parallel . . . . .	46
4.1.5	xtp_dump . . . . .	46
4.1.6	xtp_update_exciton . . . . .	46
4.1.7	xtp_basisset . . . . .	46
4.1.8	xtp_makeauxbasis . . . . .	47
4.2	Calculators . . . . .	47
4.3	Common options . . . . .	47
	<b>Bibliography</b>	<b>49</b>

# Chapter 1

## Introduction

sec:introduction

Charge carrier dynamics in an organic semiconductor can often be described in terms of charge hopping between localized states. The hopping rates depend on **electronic coupling elements**, **reorganization energies**, and **site energies**, which vary as a function of position and orientation of the molecules. The purpose of the VOTCA-XTP package [1] is to simplify the workflow for charge transport simulations, provide a uniform error-control for the methods, flexible platform for their development, and eventually allow *in silico* prescreening of organic semiconductors for specific applications.

The toolkit is implemented using modular concepts introduced earlier in the Versatile Object-oriented Toolkit for Coarse-graining Applications (VOTCA) [2]. It contains different **programs**, which execute specific tasks implemented in **calculators** representing an individual step in the workflow. Figure 1.1 summarizes a typical chain of commands to perform a charge transport simulation: First, the VOTCA code structures are adapted to reading atomistic trajectories, mapping them onto conjugated segments and rigid fragments, and substituting (if needed) rigid fragments with the optimized copies (`xtp_map`). The programs `xtp_run` and `xtp_parallel` (for heavy-duty tasks) are then used to calculate all bimolecular charge hopping rates (via precalculation of all required ingredients). **Site energies (or energetic disorder)** can be determined as a combination of internal (ionization potentials/electron affinities of single molecules) as well as electrostatic and polarization contributions within the molecular environment. The calculation of **electronic coupling elements** between conjugated segments from the corresponding molecular orbitals can be performed using a **dimer-projection** technique based on **density-functional** theory (DFT). This requires explicit calculations using quantum-chemistry software for which we provide interfaces to Gaussian, Turbomole, and NWChem. Alternatively, the **molecular orbital overlap** module calculates electronic coupling elements relying on the semi-empirical INDO Hamiltonian and molecular orbitals in the format provided by the Gaussian package.

The **kinetic Monte Carlo** module reads in the neighbor list, site coordinates, and hopping rates and performs charge dynamics simulations using either periodic boundary conditions or charge sources and sinks.

The toolkit is written as a combination of modular C++ code and scripts. The data transfer between programs is implemented via a state file (sql database), which is also used to restart simulations. Analysis functions and most of the calculation routines are encapsulated by using the observer pattern [3] which allows the implementation of new functions as individual modules.

In the following chapter 2, we summarize the **theoretical background** of the workflow of charge transport simulations and in particular its individual steps. Chapter 3 describes the structure and content of input and output files, while a full reference of **programs** and **calculators** is available in chapter 4. For a hands-on tutorial, the reader is referred to the VOTCA-XTP project page at <http://code.google.com/p/votca-xtp/>.

**Input files:**

conf.gro  
GROMACS trajectory  
topol.tpr  
GROMACS topology  
map.xml  
mapping and energies  
options.xml  
options for calculators

**Output files:**

state.sql  
sqlite3 database file for  
data transfer between  
modules



Get list of available calculators: xtp\_run/xtp\_parallel/xtp\_kmc\_run -l

Get help and list of options for a calculator: xtp\_run/xtp\_parallel/xtp\_kmc\_run -d neighborlist

Figure 1.1: A practical workflow of charge transport simulations using VOTCA-XTP. The **theoretical background** of the individual steps is given in chapter 2. Chapter 3 describes the content of input and output files, while a full reference of **programs** and **calculators** is available in chapter 4.

fig:summary

## Chapter 2

# Theoretical background

## 2.1 Workflow

A typical workflow of charge transport simulations is depicted in figure 2.1. The first step is the simulation of an atomistic morphology, which is then partitioned on hopping sites. The coordinates of the hopping sites are used to construct a list of pairs of molecules, or neighbor list.



Figure 2.1: Workflow for microscopic simulations of charge transport.

For each pair an electronic coupling element, a reorganization energy, a driving force, and eventually the hopping rate are evaluated. The neighbor list and hopping rates define a directed graph. The corresponding master equation is solved using the kinetic Monte Carlo method, which allows to explicitly monitor the charge dynamics in the system as well as to calculate time or ensemble averages of occupation probabilities, charge fluxes, correlation functions, and field-dependent mobilities.

## 2.2 Material morphology

There is no generic recipe on how to predict a large-scale atomistically-resolved morphology of an organic semiconductor. The required methods are system-specific: for ultra-pure crystals, for



Figure 2.2: The concept of conjugated segments and rigid fragments. Dashed lines indicate conjugated segments while colors denote rigid fragments. (a) Hexabenzocoronene: the  $\pi$ -conjugated system is both a rigid fragment and a conjugated segment. (b)  $\text{Alq}_3$ : the Al atom and each ligand are rigid fragments while the whole molecule is a conjugated segment. (c) Polythiophene: each repeat unit is a rigid fragment. A conjugated segment consists of one or more rigid fragments. One molecule can have several conjugated segments.

fig:segment

example, density-functional methods can be used provided the crystal structure is known from experiment. For partially disordered organic semiconductors, however, system sizes much larger than a unit cell are required. Classical molecular dynamics or Monte Carlo techniques are then the methods of choice.

In molecular dynamics, atoms are represented by point masses which interact via empirical potentials prescribed by a force-field. Force-fields are parametrized for a limited set of compounds and their refinement is often required for new molecules. In particular, special attention shall be paid to torsion potentials between successive repeat units of conjugated polymers or between functional groups and the  $\pi$ -conjugated system. First-principles methods can be used to characterize the missing terms of the potential energy function.

Self-assembling materials, such as soluble oligomers, discotic liquid crystals, block copolymers, partially crystalline polymers, etc., are the most complicated to study. The morphology of such systems often has several characteristic length scales and can be kinetically arrested in a thermodynamically non-equilibrium state. For such systems, the time- and length-scales of atomistic simulations might be insufficient to equilibrate or sample desired morphologies. In this case, systematic coarse-graining can be used to enhance sampling [2]. Note that the coarse-grained representation must reflect the structure of the atomistic system and allow for back-mapping to the atomistic resolution.

Here we assume that the morphology is already known, that is we know how the topology and the coordinates of all atoms in the systems at a given time. VOTCA-XTP can read standard GROMACS topology files. Custom definitions of **atomistic topology** via XML files are also possible. Since the description of the atomistic topology is the first step in the charge transport simulations, it is important to follow simple conventions on how the system is partitioned on molecules, residues, and how atoms are named in the topology. Required input files are described in section **atomistic topology**.

## 2.3 Conjugated segments and rigid fragments

sec:segments

With the morphology at hand, the next step is partitioning the system on hopping sites, or conjugated segments, and calculating charge transfer rates between them. Physically intuitive arguments can be used for the partitioning, which reflects the localization of the wave function of a charge. For most organic semiconductors, the molecular architecture includes relatively rigid, planar  $\pi$ -conjugated systems, which we will refer to as rigid fragments. A conjugated segment can contain one or more of such rigid fragments, which are linked by bonded degrees of freedom.



The dynamics of these degrees of freedom evolves on timescales much slower than the frequency of the internal promoting mode. In some cases, e.g. glasses, it can be ‘frozen’ due to non-bonded interactions with the surrounding molecules.

To illustrate the concept of conjugated segments and rigid fragments, three representative molecular architectures are shown in figure 2.2. The first one is a typical discotic liquid crystal, hexabenzocoronene. It consists of a conjugated core to which side chains are attached to aid self-assembly and solution processing. In this case the orbitals localized on side chains do not participate in charge transport and the conjugated  $\pi$ -system is both, a rigid fragment and a conjugated segment. In  $\text{Alq}_3$ , a metal-coordinated compound, a charge carrier is delocalized over all three ligands. Hence, the whole molecule is one conjugated segment. Individual ligands are relatively rigid, while energies of the order of  $k_B T$  are sufficient to reorient them with respect to each other. Thus the Al atom and the three ligands are rigid fragments. In the case of a conjugated polymer, one molecule can consist of several conjugated segments, while each backbone repeat unit is a rigid fragment. Since the conjugation along the backbone can be broken due to large out-of-plane twists between two repeat units, an empirical criterion, based on the dihedral angle, can be used to partition the backbone on conjugated segments [4]. However, such intuitive partitioning is, to some extent, arbitrary and shall be validated by other methods [5–7].

After partitioning, an additional step is often required to remove bond length fluctuations introduced by molecular dynamics simulations, since they are already integrated out in the derivation of the rate expression. This is achieved by substituting respective molecular fragments with rigid, planar  $\pi$ -systems optimized using first-principles methods. Centers of mass and gyration tensors are used to align rigid fragments, though a custom definition of local axes is also possible. Such a procedure also minimizes discrepancies between the force-field and first-principles-based ground state geometries of conjugated segments, which might be important for calculations of electronic couplings, reorganization energies, and intramolecular driving forces.

To partition the system on hopping sites and substitute rigid fragments with the corresponding ground-state geometries `xtp_map` program is used:

 **Mapping the GROMACS trajectory**  
`| xtp_map -t topol.tpr -c traj.xtc -s map.xml -f state.sql`

It reads in the GROMACS topology (`topol.tpr`) and trajectory (`traj.xtc`) files, definitions of conjugated segments and rigid fragments (`map.xml`) and outputs coordinates of conjugated segments (hopping sites) and rigid fragments (as provided in the MD trajectory and after rigidification) to the state file (`state.sql`). In order to do this, a mapping file `map.xml` has to be provided, which specifies the corresponding atoms in the different representations. After this step, all information (frame number, dimensions of the simulation box, etc) are stored in the state file and only this file is used for further calculations.



#### Be careful!

VOTCA-XTP requires a wrapped trajectory for mapping the segments and fragments, so all molecules should be whole in the frame.

In order to visually check the mapping one can use either the `tdump` calculator or the program `xtp_dump` with the calculator `trajectory2pdb`.

 **Writing a mapped trajectory with `xtp_dump`**  
`| xtp_dump -f state.sql -e trajectory2pdb`

122 It reads in the state file created by `xtp_map` and outputs two trajectory files corresponding to  
 123 the original and rigidified atom coordinates. To check the mapping, it is useful to superimpose  
 124 the three outputs (original atomistic, atomistic stored in the state file, and rigidified according to  
 125 ground state geometries), e.g., with VMD.

sec:tdump

 **Writing a mapped trajectory with `tdump`**  
 | `xtp_run -f state.sql -o options.xml -e tdump`

126 It also reads in the state file but appends the coordinates to a `pdb` file. So make sure to delete old  
 127 `QM.pdb` and `MD.pdb` if you want to create a new imagef

## 128 2.4 Neighbor list

sec:neighborlist

129 A list of neighboring conjugated segments, or neighbor list, contains all pairs of conjugated seg-  
 130 ments for which `coupling elements`, `reorganization energies`, `site energy differences`, and `rates`  
 131 are evaluated.

132 Two segments are added to this list if the distance between centers of mass of any of their rigid  
 133 fragments is below a certain cutoff. This allows neighbors to be selected on a criterion of min-  
 134 imum distance of approach rather than center of mass distance, which is useful for molecules  
 135 with anisotropic shapes.

136 The neighbor list can be generated from the atomistic trajectory by using the `neighborlist`  
 137 `calculator`. This calculator requires a cutoff, which can be specified in the `options.xml` file. The  
 138 list is saved to the `state.sql` file:

 **Generating a neighbor list**  
 | `xtp_run -o options.xml -f state.sql -e neighborlist`

## 139 2.5 Reorganization energy

sec:reorganization

140 The reorganization energy  $\lambda_{ij}$  takes into account the change in nuclear (and dielectric) degrees of  
 141 freedom as the charge moves from donor  $i$  to acceptor  $j$ . It has two contributions: intramolecular,  
 142  $\lambda_{ij}^{\text{int}}$ , which is due to reorganization of nuclear coordinates of the two molecules forming the  
 143 charge transfer complex, and intermolecular (outersphere),  $\lambda_{ij}^{\text{out}}$ , which is due to the relaxation of  
 144 the nuclear coordinates of the environment. In what follows we discuss how these contributions  
 145 can be calculated.

### 146 2.5.1 Intramolecular reorganization energy

sec:intramolecular

147 If intramolecular vibrational modes of the two molecules are treated classically, the rearrange-  
 148 ment of their nuclear coordinates after charge transfer results in the dissipation of the internal  
 149 reorganization energy,  $\lambda_{ij}^{\text{int}}$ . It can be computed from four points on the potential energy surfaces  
 150 (PES) of both molecules in neutral and charged states, as indicated in figure 2.3.

151 Adding the contributions due to discharging of molecule  $i$  and charging of molecule  $j$  yields [8]

$$\lambda_{ij}^{\text{int}} = \lambda_i^{cn} + \lambda_j^{nc} = U_i^{nC} - U_i^{nN} + U_j^{cN} - U_j^{cC}. \quad (2.1)$$

equ:lambda

152 Here  $U_i^{nC}$  is the internal energy of the neutral molecule  $i$  in the geometry of its charged state  
 153 (small  $n$  denotes the state and capital  $C$  the geometry). Similarly,  $U_j^{cN}$  is the energy of the charged  
 154 molecule  $j$  in the geometry of its neutral state. Note that the PES of the donor and acceptor are  
 155 not identical for chemically different compounds or for conformers of the same molecule. In this



Figure 2.3: Potential energy surfaces of (a) donor and (b) acceptor in charged and neutral states. After the change of the charge state both molecules relax their nuclear coordinates. If all vibrational modes are treated classically, the total internal reorganization energy and the internal energy difference of the electron transfer reaction are  $\lambda_{ij}^{\text{int}} = \lambda_i^{cn} + \lambda_j^{nc}$  and  $\Delta E_{ij}^{\text{int}} = \Delta U_i - \Delta U_j$ , respectively.

fig:parabolas

case  $\lambda_i^{cn} \neq \lambda_j^{cn}$  and  $\lambda_i^{nc} \neq \lambda_j^{nc}$ . Thus  $\lambda_{ij}^{\text{int}}$  is a property of the charge transfer complex, and not of a single molecule.

Intramolecular reorganization energies for discharging ( $\lambda^{cn}$ ) and charging ( $\lambda^{nc}$ ) of a molecule need to be determined using quantum-chemistry and given in `map.xml`. The values are written to the `state.sql` using the calculator `einternal` (see also internal energy):

#### Intramolecular reorganization energies

```
| xtp_run -o options.xml -f state.sql -e einternal
```

## 2.5.2 Outersphere reorganization energy

161

sec:outersphere

During the charge transfer reaction, also the molecules outside the charge transfer complex reorient and polarize in order to adjust for changes in electric potential, resulting in the outersphere contribution to the reorganization energy.  $\lambda_{ij}^{\text{out}}$  is particularly important if charge transfer occurs in a polarizable environment. Assuming that charge transfer is much slower than electronic polarization but much faster than nuclear rearrangement of the environment,  $\lambda_{ij}^{\text{out}}$  can be calculated from the electric displacement fields created by the charge transfer complex [9]

$$\lambda_{ij}^{\text{out}} = \frac{c_p}{2\epsilon_0} \int_{V^{\text{out}}} dV \left[ \vec{D}_I(\vec{r}) - \vec{D}_F(\vec{r}) \right]^2, \quad (2.2)$$

equ:lambda\_outer1

where  $\epsilon_0$  is the permittivity of free space,  $\vec{D}_{I,F}(\vec{r})$  are the electric displacement fields created by the charge transfer complex in the initial (charge on molecule  $i$ ) and final (charge transferred to molecule  $j$ ) states,  $V^{\text{out}}$  is the volume outside the complex, and  $c_p = \frac{1}{\epsilon_{\text{opt}}} - \frac{1}{\epsilon_s}$  is the Pekar factor, which is determined by the low ( $\epsilon_s$ ) and high ( $\epsilon_{\text{opt}}$ ) frequency dielectric permittivities.

Eq. (2.2) can be simplified by assuming spherically symmetric charge distributions on molecules  $i$  and  $j$  with total charge  $e$ . Integration over the volume  $V^{\text{out}}$  outside of the two spheres of radii  $R_i$  and  $R_j$  centered on molecules  $i$  and  $j$  leads to the classical Marcus expression for the outersphere reorganization energy

$$\lambda_{ij}^{\text{out}} = \frac{c_p e^2}{4\pi\epsilon_0} \left( \frac{1}{2R_i} + \frac{1}{2R_j} - \frac{1}{r_{ij}} \right), \quad (2.3)$$

equ:lambda\_outer2

where  $r_{ij}$  is the molecular separation. While eq. (2.3) captures the main physics, e.g. predicts smaller outer-sphere reorganization energies (higher rates) for molecules at smaller separations,

178 it often cannot provide quantitative estimates, since charge distributions are rarely spherically  
179 symmetric.

180 Alternatively, the displacement fields can be constructed using the atomic partial charges. The  
181 difference of the displacement fields at the position of an atom  $b_k$  outside the charge transfer  
182 complex (molecule  $k \neq i, j$ ) can be expressed as

$$\vec{D}_I(\vec{r}_{b_k}) - \vec{D}_F(\vec{r}_{b_k}) = \sum_{a_i} \frac{q_{a_i}^c - q_{a_i}^n}{4\pi} \frac{(\vec{r}_{b_k} - \vec{r}_{a_i})}{|\vec{r}_{b_k} - \vec{r}_{a_i}|^3} + \sum_{a_j} \frac{q_{a_j}^n - q_{a_j}^c}{4\pi} \frac{(\vec{r}_{b_k} - \vec{r}_{a_j})}{|\vec{r}_{b_k} - \vec{r}_{a_j}|^3}, \quad (2.4)$$

183 where  $q_{a_i}^n$  ( $q_{a_i}^c$ ) is the partial charge of atom  $a$  of the neutral (charged) molecule  $i$  in vacuum. The  
184 partial charges of neutral and charged molecules are obtained by fitting their values to reproduce  
185 the electrostatic potential of a single molecule (charged or neutral) in vacuum. Assuming a uni-  
186 form density of atoms, the integration in eq. (2.2) can be rewritten as a density-weighted sum  
187 over all atoms excluding those of the charge transfer complex.

188 The remaining unknown needed to calculate  $\lambda_{ij}^{\text{out}}$  is the Pekar factor,  $c_p$ . In polar solvents  $\epsilon_s \gg$   
189  $\epsilon_{\text{opt}} \sim 1$  and  $c_p$  is of the order of 1. In most organic semiconductors, however, molecular orien-  
190 tations are fixed and therefore the low frequency dielectric permittivity is of the same order of  
191 magnitude as  $\epsilon_{\text{opt}}$ . Hence,  $c_p$  is small and its value is very sensitive to differences in the permit-  
192 tivities.

193 Outersphere reorganization energies for all pairs of molecules in the `neighbor list` can be com-  
194 puted from the atomistic trajectory by using the `eoutersphere calculator`.

195 Two methods can be used to compute  $\lambda_{ij}^{\text{out}}$ . The first method uses the atomistic partial charges of  
196 neutral and charged molecules from files specified in `map.xml` and eq. (2.2). The Pekar factor  $c_p$   
197 and a cutoff radius based on molecular centers of mass have to be specified in the `options.xml`  
198 file.

199 If this method is computationally prohibitive,  $\lambda_{ij}^{\text{out}}$  can be computed using eq. (2.3), which as-  
200 sumes spherical charge distributions on the molecules. In this case the radii of these spheres are  
201 specified in `segments.xml`, while the Pekar factor  $c_p$  is given in the `options.xml` file and no  
202 cutoff radius is needed.

203 The outer sphere reorganization energies are saved to the `state.sql` file:

```

 Outersphere reorganization energy
| xtp_run -o options.xml -f state.sql -e outersphere

```

## 204 2.6 Site energies

sec:site\_energies

205 A charge transfer reaction between molecules  $i$  and  $j$  is driven by the site energy difference,  
206  $\Delta E_{ij} = E_i - E_j$ . Since the transfer rate,  $\omega_{ij}$ , depends exponentially on  $\Delta E_{ij}$  (see eq. (2.31)) it is  
207 important to compute its distribution as accurately as possible. The total site energy difference  
208 has contributions due to **externally applied electric field**, electrostatic interactions, polarization  
209 effects, and **internal energy** differences. In what follows we discuss how to estimate these contri-  
210 butions by making use of first-principles calculations and polarizable force-fields.

### 211 2.6.1 Externally applied electric field

sec:ext\_field

212 The contribution to the total site energy difference due to an external electric field  $\vec{F}$  is given by  
213  $\Delta E_{ij}^{\text{ext}} = q\vec{F} \cdot \vec{r}_{ij}$ , where  $q = \pm e$  is the charge and  $\vec{r}_{ij} = \vec{r}_i - \vec{r}_j$  is a vector connecting molecules  
214  $i$  and  $j$ . For typical distances between small molecules, which are of the order of 1 nm, and  
215 moderate fields of  $F < 10^8$  V/m this term is always smaller than 0.1 eV.

## 2.6.2 Internal energy

The contribution to the site energy difference due to different internal energies (see figure 2.3) can be written as

$$\Delta E_{ij}^{\text{int}} = \Delta U_i - \Delta U_j = (U_i^{cC} - U_i^{nN}) - (U_j^{cC} - U_j^{nN}), \quad (2.5)$$

where  $U_i^{cC(nN)}$  is the total energy of molecule  $i$  in the charged (neutral) state and geometry.  $\Delta U_i$  corresponds to the adiabatic ionization potential (or electron affinity) of molecule  $i$ , as shown in figure 2.3. For one-component systems and negligible conformational changes  $\Delta E_{ij}^{\text{int}} = 0$ , while it is significant for donor-acceptor systems.

Internal energies determined using quantum-chemistry need to be specified in `map.xml`. The values are written to the `state.sql` using the calculator `einternal` (see also `intramolecular reorganization energy`):

```
Internal energies
| xtp_run -o options.xml -f state.sql -e einternal
```

## 2.6.3 Electrostatic interaction energy

We represent the molecular charge density by choosing multiple expansion sites (“polar sites”) per molecule in such a way as to accurately reproduce the molecular electrostatic potential (ESP), with a set of suitably chosen multipole moments  $\{Q_{lk}^a\}$  (in spherical-tensor notation) allocated to each site. The expression for the electrostatic interaction energy between two molecules  $A$  and  $B$  in the multi-point expansion includes an implicit sum over expansion sites  $a \in A$  and  $b \in B$ ,

$$U_{AB} = \sum_{a \in A} \sum_{b \in B} \hat{Q}_{l_1 k_1}^a T_{l_1 k_1 l_2 k_2}^{a,b} \hat{Q}_{l_2 k_2}^b \equiv \hat{Q}_{l_1 k_1}^a T_{l_1 k_1 l_2 k_2}^{a,b} \hat{Q}_{l_2 k_2}^b, \quad (2.6)$$

where we have used the Einstein sum convention for the site indices  $a$  and  $b$  on the right-hand side of the equation, in addition to the sum convention that is in place for the multipole-moment components  $t \equiv l_1 k_1$  and  $u \equiv l_2 k_2$ . The  $T_{l_1 k_1 l_2 k_2}^{a,b}$  are tensors that mediate the interaction between a multipole component  $l_1 k_1$  on site  $a$  with the moment  $l_2 k_2$  on site  $b$ . If we include the molecular environment into a perturbative term  $W$  to enter in the single-molecule Hamiltonian, the above expression is exactly the first-order correction to the energy where the quantum-mechanical detail has been absorbed in classical multipole moments.

There are a number of strategies how to arrive at such a collection of *distributed multipoles*. They can be classified according to whether the multipoles are derived (a) from the electrostatic potential generated by the SCF charge density or (b) from a decomposition of the wavefunction itself. Here, we will only draft two of those approaches, CHELPG [10] from category (a) and DMA [11] from category (b).

The CHELPG (CHarges from ELEctrostatic Potentials, Grid-based) method relies on performing a least-squares fit of atom-placed charges to reproduce the electrostatic potential as evaluated from the SCF density on a regularly spaced grid [10]. The fitted charges result from minimizing the Lagrangian function [12]

$$z(\{q_i\}) = \sum_{k=1}^M \left( \phi(\vec{r}_k) - \sum_{i=1}^N \frac{1}{4\pi\epsilon_0} \frac{q_i}{|\vec{r}_i - \vec{r}_k|} \right) + \lambda \left( q_{\text{mol}} - \sum_{i=1}^N q_i \right), \quad (2.7)$$

with  $M$  grid points,  $N$  atomic sites, the set of atomic partial charges  $\{q_i\}$  and the SCF potential  $\phi$ . The Lagrange multiplier  $\lambda$  constrains the sum of the fitted charges to the molecular charge  $q_{\text{mol}}$ . The main difference from other fitting schemes [13] is the algorithm that selects the positions

at which the potential is evaluated (we note that the choice of grid points can have substantial effects especially for bulky molecules). Clearly, the CHELPG method can be (and has been) extended to include higher atomic multipoles. It should be noted, however, how already the inclusion of atomic dipoles hardly improves the parametrization, and can in fact be harmful to its conformational stability.

The Distributed-Multipole-Analysis (DMA) approach [11, 14], developed by A. Stone, operates directly on the quantum-mechanical density matrix, expanded in terms of atom- and bond-centered Gaussian functions  $\chi_\alpha = R_{LK}(\vec{x} - \vec{s}_\alpha) \exp[-\zeta(\vec{x} - \vec{s}_\alpha)^2]$ ,

$$\rho(\vec{x}) = \sum_{\alpha,\beta} \rho_{\alpha\beta} \chi_\alpha(\vec{x} - \vec{s}_\alpha) \chi_\beta(\vec{x} - \vec{s}_\beta). \quad (2.8)$$

The aim is to compute multipole moments according in a distributed fashion: If we use that the overlap product  $\chi_\alpha \chi_\beta$  of two Gaussian basis functions yields itself a Gaussian centered at  $\vec{P} = (\zeta_\alpha \vec{s}_\alpha + \zeta_\beta \vec{s}_\beta) / (\zeta_\alpha + \zeta_\beta)$ , it is possible to proceed in two steps: First, we compute the multipole moments associated with a specific summand in the density matrix, referred to the overlap center  $\vec{P}$ :

$$Q_{LK}[\vec{P}] = - \int R_{LK}(\vec{x} - \vec{P}) \rho_{\alpha\beta} \chi_\alpha \chi_\beta d^3x. \quad (2.9)$$

Second, we transfer the resulting  $Q_{lk}[\vec{P}]$  to the position  $\vec{S}$  of a polar site according to the rule [11]

$$Q_{nm}[\vec{S}] = \sum_{l=0}^L \sum_{k=-l}^l \left[ \binom{n+m}{l+k} \binom{n-m}{l-k} \right]^{1/2} R_{n-l,m-k}(\vec{S} - \vec{P}) \cdot Q_{lk}[\vec{P}]. \quad (2.10)$$

Note how this requires a rule for the choice of the expansion site to which the multipole moment should be transferred. In the near past [14], the nearest-site algorithm, which allocates the multipole moments to the site closest to the overlap center, was replaced for diffuse functions by an algorithm based on a sxtptth weighting function in conjunction with grid-based integration methods in order to decrease the basis-set dependence of the resulting set of distributed multipoles. One important advantage of the DMA approach over fitting algorithms such as CHELPG or Merz-Kollman (MK) is that higher-order moments can also be derived without too large an ambiguity.

The ‘mps’ file format used by VOTCA for the definition of distributed multipoles (as well as point polarizabilities, see subsequent section) is based on the GDMA punch format of A. Stone’s GDMA program [14] (the punch output file can be immediately plugged into VOTCA without any conversions to be applied). Furthermore the log-file of different QM packages (currently Gaussian, Turbomole and NWChem) may be fed into the `log2mps` tool, which will subsequently generate the appropriate mps-file.



**Read in ESP charges from a QM log file**

```
| xtp_tools -o options.xml -e log2mps
```

## 2.6.4 Induction energy - the Thole model

If we in addition to the permanent set of multipole moments  $\{Q_t^a\}$  allow for induced moments  $\{\Delta Q_t^a\}$  and penalize their generation with a bilinear form (giving rise to a strictly positive contribution to the energy),

$$U_{\text{int}} = \frac{1}{2} \sum_A \Delta Q_t^a \eta_{tt'}^{aa'} \Delta Q_{t'}^{a'}, \quad (2.11)$$



it can be shown that the induction contribution to the site energy evaluates to an expression where all interactions between induced moments have cancelled out, and interactions between permanent and induced moments are scaled down by 1/2 [15]:

$$U_{pu} = \frac{1}{2} \sum_A \sum_{B>A} [\Delta Q_t^a T_{tu}^{ab} Q_u^b + \Delta Q_t^b T_{tu}^{ab} Q_u^a]. \quad (2.12) \quad \text{equ:u\_pu}$$

This term can be viewed as the second-order (induction) correction to the molecular interaction energy. The sets of  $\{Q_t^a\}$  are solved for self-consistently via

$$\Delta Q_t^a = - \sum_{B \neq A} \alpha_{tt'}^{aa'} T_{t'u}^{a'b} (Q_u^b + \Delta Q_u^b), \quad (2.13) \quad \text{equ:self\_consistent\_dQ}$$

where the polarizability tensors  $\alpha_{tt'}^{aa'}$  are given by the inverse of  $\eta_{tt'}^{aa'}$ . With eqs. 2.13 and 2.12 we have at hand expressions that allow us to compute the induction energy contribution to site energies in an iterative manner based on a set of molecular distributed multipoles  $\{Q_t^a\}$  and polarizabilities  $\{\alpha_{tt'}^{aa'}\}$ . We have drafted in the previous section how to obtain the former from a wavefunction decomposition or fitting scheme (GDMA, CHELPG). The  $\{\alpha_{tt'}^{aa'}\}$  can be derived formally (or rather: read off) from a perturbative expansion of the molecular interaction. In this work we make use of the Thole model [16, 17] as a semi-empirical approach to obtain the sought-after point polarizabilities in the local dipole approximation, that is,  $[\alpha_{tt'}^{aa'}] = \alpha_{tt'}^{aa'} \delta_{t\beta} \delta_{t'\beta} \delta_{aa'}$ , where  $\beta \in \{x, y, z\}$  references the dipole-moment component. The Thole model is based on a modified dipole-dipole interaction, which can be reformulated in terms of the interaction of smeared charge densities. This has been shown to be necessary due to the divergent head-to-tail dipole-dipole interaction that otherwise results at small interseparations on the Å scale [16–18]. Smearing out the charge distribution mimics the nature of the QM wavefunction, which effectively guards against this unphysical polarization catastrophe. Since the point dipoles however only react individually to the external field, any correlation effects as were still accounted for in the  $\{\alpha_{tt'}^{aa'}\}$  are lost, except perhaps those correlations that are due to the mere classical field interaction.

The smearing of the nuclei-centered multipole moments is obtained via a fractional charge density  $\rho_f(\vec{u})$  which should be normalized to unity and fall off rapidly as of a certain radius  $\vec{u} = \vec{u}(\vec{R})$ . The latter is related to the physical distance vector  $\vec{R}$  connecting two interacting sites via a linear scaling factor that takes into account the magnitude of the isotropic site polarizabilities  $\alpha^a$ . This isotropic fractional charge density gives rise to a modified potential

$$\phi(u) = -\frac{1}{4\pi\epsilon_0} \int_0^u 4\pi u' \rho(u') du' \quad (2.14) \quad \text{equ:mod\_potential}$$

We can relate the multipole interaction tensor  $T_{ij\dots}$  (this time in Cartesian coordinates) to the fractional charge density in two steps: First, we rewrite the tensor in terms of the scaled distance vector  $\vec{u}$ ,

$$T_{ij\dots}(\vec{R}) = f(\alpha^a \alpha^b) t_{ij\dots}(\vec{u}(\vec{R}), \alpha^a \alpha^b), \quad (2.15)$$

where the specific form of  $f(\alpha^a \alpha^b)$  results from the choice of  $u(\vec{R}, \alpha^a \alpha^b)$ . Second, we demand that the smeared interaction tensor  $t_{ij\dots}$  is given as usual by the appropriate derivative of the potential in eq. 2.14,

$$t_{ij\dots}(\vec{u}) = -\partial_{u_i} \partial_{u_j} \dots \phi(\vec{u}). \quad (2.16)$$

It turns out that for a suitable choice of  $\rho_f(\vec{u})$ , the modified interaction tensors can be rewritten in such a way that powers  $n$  of the distance  $R = |\vec{R}|$  are damped with a damping function  $\lambda_n(\vec{u}(\vec{R}))$  [19].

There is a large number of fractional charge densities  $\rho_f(\vec{u})$  that have been tested for the purpose of giving best results for the molecular polarizability as well as interaction energies. Note how a great advantage of the Thole model is the exceptional transferability of the atomic polarizabilities to compounds not used for the fitting procedure [17]. In fact, for most organic molecules, a fixed set of atomic polarizabilities ( $\alpha_C = 1.334$ ,  $\alpha_H = 0.496$ ,  $\alpha_N = 1.073$ ,  $\alpha_O = 0.873$ ,  $\alpha_S = 2.926 \text{ \AA}^3$ ) based on atomic elements yields satisfactory results.

VOTCA implements the Thole model with an exponentially-decaying fractional charge density

$$\rho(u) = \frac{3a}{4\pi} \exp(-au^3), \quad (2.17)$$

where  $\vec{u}(\vec{R}, \alpha^a \alpha^b) = \vec{R}/(\alpha^a \alpha^b)^{1/6}$  and the smearing exponent  $a = 0.39$  (which can however be changed from the program options), as used in the AMOEBA force field [19].

Even though the Thole model performs very well for many organic compounds with only the above small set of element-based polarizabilities, conjugated molecules may require a more intricate parametrization. The simplest approach is to resort to scaled polarizabilities to match the effective molecular polarizable volume  $V \sim \alpha_x \alpha_y \alpha_z$  as predicted by QM calculations (here  $\alpha_x, \alpha_y, \alpha_z$  are the eigenvalues of the molecular polarizability tensor). The `molpol` tool assists with this task, it self-consistently calculates the Thole polarizability for an input `mps`-file and optimizes (if desired) the atomic polarizabilities in the above simple manner.

#### Generate Thole-type polarizabilities for a segment

```
| xtp_tools -o options.xml -e molpol
```

The electrostatic and induction contribution to the site energy is evaluated by the `emultipole` calculator. Atomistic partial charges for charged and neutral molecules are taken from `mps`-files (extended GDMA format) specified in `map.xml`. Note that, in order to speed up calculations for both methods, a cut-off radius (for the molecular centers of mass) can be given in `options.xml`. Threaded execution is advised.

#### Electrostatic and induction corrections

```
| xtp_run -o options.xml -f state.sql -e emultipole
```

Furthermore available are `zmultipole`, which extends `emultipole` to allow for an electrostatic buffer layer (loosely related to the z-buffer in OpenGL, hence the name) and anisotropic point polarizabilities. For the interaction energy of charged clusters of any user-defined composition (Frenkel states, CT states, ...), `xqmultipole` can be used.

#### Interaction energy of charged molecular clusters embedded in a molecular environment

```
| xtp_parallel -o options.xml -f state.sql -e xqmultipole
```

## 2.7 Transfer integrals

The electronic transfer integral element  $J_{ij}$  entering the Marcus rates in eq. (2.31) is defined as

$$J_{ij} = \langle \phi_i | \hat{H} | \phi_j \rangle, \quad (2.18) \quad \text{equ:TI}$$

where  $\phi_i$  and  $\phi_j$  are diabatic wavefunctions, localized on molecule  $i$  and  $j$  respectively, participating in the charge transfer, and  $\hat{H}$  is the Hamiltonian of the formed dimer. Within the frozen-core approximation, the usual choice for the diabatic wavefunctions  $\phi_i$  is the highest occupied molecular orbital (HOMO) in case of hole transport, and the lowest unoccupied molecular orbital (LUMO) in the case of electron transfer, while  $\hat{H}$  is an effective single particle Hamiltonian,



e.g. Fock or Kohn-Sham operator of the dimer. As such,  $J_{ij}$  is a measure of the strength of the electronic coupling of the frontier orbitals of monomers mediated by the dimer interactions. Intrinsically, the transfer integral is very sensitive to the molecular arrangement, i.e. the distance and the mutual orientation of the molecules participating in charge transport. Since this arrangement can also be significantly influenced by static and/or dynamic disorder [20–24], it is essential to calculate  $J_{ij}$  explicitly for each hopping pair within a realistic morphology. Considering that the number of dimers for which eq. (2.18) has to be evaluated is proportional to the number of molecules times their coordination number, computationally efficient and at the same time quantitatively reliable schemes are required.

### 2.7.1 Projection of monomer orbitals on dimer orbitals (DIPRO)

sec:dipro

An approach for the determination of the transfer integral that can be used for any single-particle electronic structure method (Hartree-Fock, DFT, or semiempirical methods) is based on the projection of monomer orbitals on a manifold of explicitly calculated dimer orbitals. This dimer projection (DIPRO) technique including an assessment of computational parameters such as the basis set, exchange-correlation functionals, and convergence criteria is presented in detail in ref. [25]. A brief summary of the concept is given below.

We start from an effective Hamiltonian<sup>1</sup>

$$\hat{H}^{\text{eff}} = \sum_i \epsilon_i \hat{a}_i^\dagger \hat{a}_i + \sum_{j \neq i} J_{ij} \hat{a}_i^\dagger \hat{a}_j + c.c. \quad (2.19) \quad \text{equ:dipro\_eq1}$$

where  $\hat{a}_i^\dagger$  and  $\hat{a}_i$  are the creation and annihilation operators for a charge carrier located at the molecular site  $i$ . The electron site energy is given by  $\epsilon_i$ , while  $J_{ij}$  is the transfer integral between two sites  $i$  and  $j$ . We label their frontier orbitals (HOMO for hole transfer, LUMO for electron transfer)  $\phi_i$  and  $\phi_j$ , respectively. Assuming that the frontier orbitals of a dimer (adiabatic energy surfaces) result exclusively from the interaction of the frontier orbitals of monomers, and consequently expand them in terms of  $\phi_i$  and  $\phi_j$ . The expansion coefficients,  $\bar{\mathbf{C}}$ , can be determined by solving the secular equation

$$(\mathbf{H} - E\mathbf{S})\bar{\mathbf{C}} = 0 \quad (2.20) \quad \text{equ:dipro\_eq2}$$

where  $\mathbf{H}$  and  $\mathbf{S}$  are the Hamiltonian and overlap matrices of the system, respectively. These matrices can be written explicitly as

$$\mathbf{H} = \begin{pmatrix} e_i & H_{ij} \\ H_{ij}^* & e_j \end{pmatrix} \quad \mathbf{S} = \begin{pmatrix} 1 & S_{ij} \\ S_{ij}^* & 1 \end{pmatrix} \quad (2.21) \quad \text{equ:dipro\_eq3}$$

with

$$\begin{aligned} e_i &= \langle \phi_i | \hat{H} | \phi_i \rangle & H_{ij} &= \langle \phi_i | \hat{H} | \phi_j \rangle \\ e_j &= \langle \phi_j | \hat{H} | \phi_j \rangle & S_{ij} &= \langle \phi_j | \phi_j \rangle \end{aligned} \quad (2.22) \quad \text{equ:dipro\_eq4}$$

The matrix elements  $e_{i(j)}$ ,  $H_{ij}$ , and  $S_{ij}$  entering eq. (2.21) can be calculated via projections on the dimer orbitals (eigenfunctions of  $\hat{H}$ )  $\{|\phi_n^D\rangle\}$  by inserting  $\hat{1} = \sum_n |\phi_n^D\rangle \langle \phi_n^D|$  twice. We exemplify this explicitly for  $H_{ij}$  in the following

$$H_{ij} = \sum_{nm} \langle \phi_i | \phi_n^D \rangle \langle \phi_n^D | \hat{H} | \phi_m^D \rangle \langle \phi_m^D | \phi_j \rangle. \quad (2.23) \quad \text{equ:dipro\_eq16}$$

The Hamiltonian is diagonal in its eigenfunctions,  $\langle \phi_n^D | \hat{H} | \phi_m^D \rangle = E_n \delta_{nm}$ . Collecting the projections of the frontier orbitals  $|\phi_{i(j)}\rangle$  on the  $n$ -th dimer state  $(\bar{\mathbf{V}}_{(i)})_n = \langle \phi_i | \phi_n^D \rangle$  and  $(\bar{\mathbf{V}}_{(j)})_n = \langle \phi_j | \phi_n^D \rangle$  respectively, into vectors we obtain

$$H_{ij} = \bar{\mathbf{V}}_{(i)} \mathbf{E} \bar{\mathbf{V}}_{(j)}^\dagger. \quad (2.24) \quad \text{equ:dipro\_eq17}$$

<sup>1</sup>we use following notations:  $a$  - number,  $\bar{\mathbf{a}}$  - vector,  $\mathbf{A}$  - matrix,  $\hat{A}$  - operator

What is left to do is determine these projections  $\bar{\mathbf{V}}_{(k)}$ . In all practical calculations the molecular orbitals are expanded in basis sets of either plane waves or of localized atomic orbitals  $|\varphi_\alpha\rangle$ . We will first consider the case that the calculations for the monomers are performed using a counterpoise basis set that is commonly used to deal with the basis set superposition error (BSSE). The basis set of atom-centered orbitals of a monomer is extended to the one of the dimer by adding the respective atomic orbitals at virtual coordinates of the second monomer. We can then write the respective expansions as

$$|\phi_k\rangle = \sum_{\alpha} \lambda_{\alpha}^{(k)} |\varphi_{\alpha}\rangle \quad \text{and} \quad |\phi_n^D\rangle = \sum_{\alpha} D_{\alpha}^{(n)} |\varphi_{\alpha}\rangle \quad (2.25) \quad \text{eq:dipro_eq18}$$

where  $k = i, j$ . The projections can then be determined within this common basis set as

$$(\bar{\mathbf{V}}_k)_n = \langle \phi_k | \phi_n^D \rangle = \sum_{\alpha} \lambda_{\alpha}^{(k)} \langle \alpha | \sum_{\beta} D_{\beta}^{(n)} |\beta\rangle = \bar{\lambda}_{(k)}^{\dagger} \mathcal{S} \bar{\mathbf{D}}_{(n)} \quad (2.26) \quad \text{eq:dipro_eq19}$$

where  $\mathcal{S}$  is the overlap matrix of the atomic basis functions. This allows us to finally write the elements of the Hamiltonian and overlap matrices in eq. (2.21) as:

$$\begin{aligned} H_{ij} &= \bar{\lambda}_{(i)}^{\dagger} \mathcal{S} \mathbf{D} \mathbf{E} \mathbf{D}^{\dagger} \mathcal{S}^{\dagger} \bar{\lambda}_{(j)} \\ S_{ij} &= \bar{\lambda}_{(i)}^{\dagger} \mathcal{S} \mathbf{D} \mathbf{D}^{\dagger} \mathcal{S}^{\dagger} \bar{\lambda}_{(j)} \end{aligned} \quad (2.27) \quad \text{eq:dipro_eq20}$$

Since the two monomer frontier orbitals that form the basis of this expansion are not orthogonal in general ( $\mathbf{S} \neq \mathbf{1}$ ), it is necessary to transform eq. (2.20) into a standard eigenvalue problem of the form

$$\mathbf{H}^{\text{eff}} \bar{\mathbf{C}}^{\text{eff}} = E \bar{\mathbf{C}}^{\text{eff}} \quad (2.28) \quad \text{eq:dipro_eq7}$$

to make it correspond to eq. (2.19). According to Löwdin such a transformation can be achieved by

$$\mathbf{H}^{\text{eff}} = \mathbf{S}^{-1/2} \mathbf{H} \mathbf{S}^{-1/2}. \quad (2.29) \quad \text{eq:dipro_eq9}$$

This then yields an effective Hamiltonian matrix in an orthogonal basis, and its entries can directly be identified with the site energies  $\epsilon_i$  and transfer integrals  $J_{ij}$ :

$$\mathbf{H}^{\text{eff}} = \begin{pmatrix} e_i^{\text{eff}} & H_{ij}^{\text{eff}} \\ H_{ij}^{*,\text{eff}} & e_j^{\text{eff}} \end{pmatrix} = \begin{pmatrix} \epsilon_i & J_{ij} \\ J_{ij}^* & \epsilon_j \end{pmatrix} \quad (2.30) \quad \text{eq:dipro_eq11}$$

## 2.7.2 DFT-based transfer integrals using DIPRO

sec:dft

The calculation of one electronic coupling element based on DFT using the DIPRO method requires the overlap matrix of atomic orbitals  $\mathcal{S}$ , the expansion coefficients for monomer  $\bar{\lambda}_{(k)} = \{\lambda_{\alpha}^{(k)}\}$  and dimer orbitals  $\bar{\mathbf{D}}_{(n)} = \{D_{\alpha}^{(n)}\}$ , as well as the orbital energies  $E_n$  of the dimer are required as input. In practical situations, performing self-consistent quantum-chemical calculations for each individual monomer and one for the dimer to obtain this input data is extremely demanding. Several simplifications can be made to reduce the computational effort, such as using non-Counterpoise basis sets for the monomers (thereby decoupling the monomer calculations from the dimer run) and performing only a single SCF step in a dimer calculation starting from an initial guess formed from a superposition of monomer orbitals. This "noCP+noSCF" variant of DIPRO is shown in figure 2.4(a) and recommended for production runs. A detailed comparative study of the different variants can be found in [25].

The code currently contains supports evaluation of transfer integrals from quantum-chemical calculations performed with the Gaussian, Turbomole, and NWChem packages. The interfacing procedure consists of three main steps: generation of input files for monomers and dimers, performing the actual quantum-chemical calculations, and calculating the transfer integrals.



Figure 2.4: Schematics of the DIPRO method. (a) General workflow of the projection technique. (b) Strategy of the efficient noCP+noSCF implementation, in which the monomer calculations are performed independently from the dimer configurations (noCP), using the `edft calculator`. The dimer Hamiltonian is subsequently constructed based on an initial guess formed from monomer orbitals and only diagonalized once (noSCF) before the transfer integral is calculated by projection. This second step is performed by the `idft calculator`.

fig:dipro\_scheme

### Monomer calculations

First, `hopping sites` and a `neighbor list` need to be generated from the atomistic topology and trajectory and written to the `state.sql` file. Then the parallel `edft calculator` manages the calculation of the monomer properties required for the determination of electronic coupling elements. Specifically, the individual steps it performs are:

1. Creation of a job file containing the list of molecules to be calculated with DFT

```

Writing job file for edft
| xtp_parallel -o options.xml -f state.sql -e edft -jwrite

```

2. Running of all jobs in job file

```

Running all edft jobs
| xtp_parallel -o options.xml -f state.sql -e edft -jrun

```

which includes

- creating the input files for the DFT calculation (using the package specified in `options.xml`) in the directory

389 OR\_FILES/package/frame\_F/mol\_M

390 where F is the index of the frame in the trajectory, M is the index of a molecule in this  
391 frame,

- 392 • executing the DFT run, and
- 393 • after completion of this run, parsing the output (number of electrons, basis set, molec-  
394 ular orbital expansion coefficients), and saving it in compressed form to

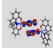
395 OR\_FILES/molecules/frame\_F/molecule\_M.orb

### 396 Calculating the transfer integrals

sec:tdft

397 After the monomer calculations have been completed successfully, the respective runs for dimers  
398 from the neighborlist can be performed using the parallel `idft` **calculator**, which manages the  
399 DFT runs for the hopping pairs and determines the coupling element using DIPRO. Again, sev-  
400 eral steps are required:

- 401 1. Creation of a job file containing the list of pairs to be calculated with DFT

 **Writing job file for idft**  
| `xtp_parallel -o options.xml -f state.sql -e idft -j write`

- 402 2. Running of all jobs in job file

 **Running all idft jobs**  
| `xtp_parallel -o options.xml -f state.sql -e idft -j run`

403 which includes

- 404 • creating the input files (including the merged guess for a noSCF calculation, if re-  
405 quested) for the DFT calculation (using the package specified in `options.xml`) in the  
406 directory

407 OR\_FILES/package/frame\_F/pair\_M\_N

408 where M and N are the indices of the molecules in this pair,

- 409 • executing the DFT run, and
- 410 • after completion of this run, parsing the output (number of electrons, basis set, molec-  
411 ular orbital expansion coefficients and energies, atomic orbital overlap matrix), and  
412 saving the pair information in compressed form to

413 OR\_FILES/pairs/frame\_F/pair\_M\_N.orb

- 414 • loading the monomer orbitals from the previously saved `*.orb` files.
- 415 • calculating the coupling elements and write them to the job file

- 416 3. Reading the coupling elements from the job file and saving them to the `state.sql` file

417

 **Saving idft results from job file to state.sql**  
| `xtp_parallel -o options.xml -f state.sql -e idft -j read`

### 2.7.3 ZINDO-based transfer integrals using MOO

An approximate method based on Zerner's Intermediate Neglect of Differential Overlap (ZINDO) has been described in Ref. [26]. This semiempirical method is substantially faster than first-principles approaches, since it avoids the self-consistent calculations on each individual monomer and dimer. This allows to construct the matrix elements of the ZINDO Hamiltonian of the dimer from the weighted overlap of molecular orbitals of the two monomers. Together with the introduction of rigid segments, only a single self-consistent calculation on one isolated conjugated segment is required. All relevant molecular overlaps can then be constructed from the obtained molecular orbitals.

The main advantage of the molecular orbital overlap (MOO) library is *fast* evaluation of electronic coupling elements. Note that MOO is based on the ZINDO Hamiltonian which has limited applicability. The general advice is to first compare the accuracy of the MOO method to the DFT-based calculations.

MOO can be used both in a standalone mode and as an `izindo` calculator of VOTCA-XTP.

Since MOO constructs the Fock operator of a dimer from the molecular orbitals of monomers by translating and rotating the orbitals of *rigid fragments*, the optimized geometry of all *conjugated segments* and the coefficients of the molecular orbitals are required as its input in addition to the state file (`state.sql`) with the *neighbor list*. Coordinates are stored in `geometry.xyz` files with four columns, first being the atom type and the next three atom coordinates. This is a standard `xyz` format without a header. Note that the atom order in the `geometry.xyz` files can be different from that of the mapping files. The correspondence between the two is established in the `map.xml` file.



#### Be careful!

Izindo requires the specification of orbitals for hole and electron transport in `map.xml`. They are the HOMO and LUMO respectively and can be retrieved from the `log` file from which the `zindo.orb` file is generated. The number of alpha electrons is the HOMO, the LUMO is HOMO+1

The calculated transfer integrals are immediately saved to the `state.sql` file.



#### Transfer integrals from `izindo`

```
| xtp_run -o options.xml -f state.sql -e izindo
```

## 2.8 Charge transfer rate

Charge transfer rates can be postulated based on intuitive physical considerations, as it is done in the Gaussian disorder models [20, 27–29]. Alternatively, charge transfer theories can be used to evaluate rates from quantum chemical calculations [1, 8, 25, 30–32]. In spite of being significantly more computationally demanding, the latter approach allows to link the chemical and electronic structure, as well as the morphology, to charge dynamics.

### 2.8.1 Classical charge transfer rate

The high temperature limit of classical charge transfer theory [33, 34] is often used as a trade-off between theoretical rigor and computational complexity. It captures key parameters which influence charge transport while at the same time providing an analytical expression for the rate. Within this limit, the transfer rate for a charge to hop from a site  $i$  to a site  $j$  reads

$$\omega_{ij} = \frac{2\pi}{\hbar} \frac{J_{ij}^2}{\sqrt{4\pi\lambda_{ij}k_B T}} \exp \left[ -\frac{(\Delta E_{ij} - \lambda_{ij})^2}{4\lambda_{ij}k_B T} \right], \quad (2.31) \quad \text{equ:marcus}$$

where  $T$  is the temperature,  $\lambda_{ij} = \lambda_{ij}^{\text{int}} + \lambda_{ij}^{\text{out}}$  is the **reorganization energy**, which is a sum of intra- and inter-molecular (outersphere) contributions,  $\Delta E_{ij}$  is the **site-energy difference**, or driving force, and  $J_{ij}$  is the **electronic coupling element**, or transfer integral.

## 2.8.2 Semi-classical bimolecular rate

The main assumptions in eq. (2.31) are non-adiabaticity (small electronic coupling and charge transfer between two diabatic, non-interacting states), and harmonic promoting modes, which are treated classically. At ambient conditions, however, the intramolecular promoting mode, which roughly corresponds to C-C bond stretching, has a vibrational energy of  $\hbar\omega \approx 0.2 \text{ eV} \gg k_B T$  and should be treated quantum-mechanically. The outer-sphere (slow) mode has much lower vibrational energy than the intramolecular promoting mode, and therefore can be treated classically. The weak interaction between molecules also implies that each molecule has its own, practically independent, set of quantum mechanical degrees of freedom. A more general, quantum-classical expression for a bimolecular multi-channel rate is derived in the Supporting Information of ref. [1] and has the following form

$$\omega_{ij} = \frac{2\pi}{\hbar} \frac{|J_{ij}|^2}{\sqrt{4\pi\lambda_{ij}^{\text{out}}k_B T}} \sum_{l', m'=0}^{\infty} |\langle \chi_{i0}^c | \chi_{il'}^n \rangle|^2 |\langle \chi_{j0}^n | \chi_{jm'}^c \rangle|^2 \exp \left\{ -\frac{[\Delta E_{ij} - \hbar(l'\omega_i^n + m'\omega_j^c) - \lambda_{ij}^{\text{out}}]^2}{4\lambda_{ij}^{\text{out}}k_B T} \right\}. \quad (2.32)$$

If the curvatures of intramolecular PES of charged and neutral states of a molecule are different, that is  $\omega_i^c \neq \omega_i^n$ , the corresponding reorganization energies,  $\lambda_i^{cn} = \frac{1}{2}[\omega_i^n(q_i^n - q_i^c)]^2$  and  $\lambda_i^{nc} = \frac{1}{2}[\omega_i^c(q_i^n - q_i^c)]^2$ , will also differ. In this case the Franck-Condon (FC) factors for discharging of molecule  $i$  read [35]

$$|\langle \chi_{i0}^c | \chi_{il'}^n \rangle|^2 = \frac{2}{2^{l'} l'! (\omega_i^c + \omega_i^n)} \exp(-|s_i|) \left[ \sum_{\substack{k=0 \\ k \text{ even}}}^{l'} \binom{l'}{k} \left( \frac{2\omega_i^c}{\omega_i^c + \omega_i^n} \right)^{k/2} \frac{k!}{(k/2)!} H_{l'-k} \left( \frac{s_i}{\sqrt{2S_i^{cn}}} \right) \right]^2, \quad (2.33)$$

where  $H_n(x)$  is a Hermite polynomial,  $s_i = 2\sqrt{\lambda_i^{nc}\lambda_i^{cn}}/\hbar(\omega_i^c + \omega_i^n)$ , and  $S_i^{cn} = \lambda_i^{cn}/\hbar\omega_i^c$ . The FC factors for charging of molecule  $j$  can be obtained by substituting  $(s_i, S_i^{cn}, \omega_i^c)$  with  $(-s_j, S_j^{nc}, \omega_j^n)$ . In order to evaluate the FC factors, the **internal reorganization energy**  $\lambda_i^{cn}$  can be computed from the intramolecular PES.

## 2.8.3 Semi-classical rate

One can also use the quantum-classical rate with a common set of vibrational coordinates [9]

$$\omega_{ij} = \frac{2\pi}{\hbar} \frac{|J_{ij}|^2}{\sqrt{4\pi\lambda_{ij}^{\text{out}}k_B T}} \sum_{N=0}^{\infty} \frac{1}{N!} \left( \frac{\lambda_{ij}^{\text{int}}}{\hbar\omega^{\text{int}}} \right)^N \exp \left( -\frac{\lambda_{ij}^{\text{int}}}{\hbar\omega^{\text{int}}} \right) \exp \left\{ -\frac{[\Delta E_{ij} - \hbar N\omega^{\text{int}} - \lambda_{ij}^{\text{out}}]^2}{4\lambda_{ij}^{\text{out}}k_B T} \right\}. \quad (2.34)$$

Numerical estimates show that if  $\lambda_{ij}^{\text{int}} \approx \lambda_{ij}^{\text{out}}$  and  $|\Delta E_{ij}| \ll \lambda_{ij}^{\text{out}}$  the rates are similar to those of eq. (2.31). In general, there is no robust method to compute  $\lambda_{ij}^{\text{out}}$  [36] and both reorganization energies are often assumed to be of the same order of magnitude. In this case the second condition also holds, unless there are large differences in electron affinities or ionization potentials of neighboring molecules, e.g. in donor-acceptor blends.

To calculate rates of the type specified in `options.xml` for all pairs in the `neighbor list` and to save them into the `state.sql` file, run the `rates calculator`. Note that all required ingredients (`reorganization energies`, `transfer integrals`, and `site energies` have to be calculated before).

 **Calculation of transfer rates**  
`| xtp_run -o options.xml -f state.sql -e rates`

## 2.9 Master equation

sec:kmc

Having determined the list of conjugated segments (hopping sites) and charge transfer rates between them, the next task is to solve the master equation which describes the time evolution of the system

$$\frac{\partial P_\alpha}{\partial t} = \sum_{\beta} P_\beta \Omega_{\beta\alpha} - \sum_{\beta} P_\alpha \Omega_{\alpha\beta}, \quad (2.35) \quad \text{equ:master}$$

where  $P_\alpha$  is the probability of the system to be in a state  $\alpha$  at time  $t$  and  $\Omega_{\alpha\beta}$  is the transition rate from state  $\alpha$  to state  $\beta$ . A state  $\alpha$  is specified by a set of site occupations,  $\{\alpha_i\}$ , where  $\alpha_i = 1(0)$  for an occupied (unoccupied) site  $i$ , and the matrix  $\hat{\Omega}$  can be constructed from rates  $\omega_{ij}$ .

The solution of eq. (2.35) is obtained by using kinetic Monte Carlo (KMC) methods. KMC explicitly simulates the dynamics of charge carriers by constructing a Markov chain in state space and can find both stationary and transient solutions of the master equation. The main advantage of KMC is that only states with a direct link to the current state need to be considered at each step. Since these can be constructed solely from current site occupations, extensions to multiple charge carriers (without the mean-field approximation), site-occupation dependent rates (needed for the explicit treatment of Coulomb interactions), and different types of interacting particles and processes, are straightforward. To optimize memory usage and efficiency, a combination of the variable step size method [37] and the first reaction method is implemented.

To obtain the dynamics of charges using KMC, the program `xtp_kmc_run` executes a specific `calculator` after reading its options (charge carrier type, runtime, number of carriers etc.) from `options.xml`.

 **KMC for a single carrier in periodic boundary conditions**  
`| xtp_kmc_run -o options.xml -f state.sql -e kmcsingle`

 **KMC for multiple carriers of the same type in periodic boundary conditions**  
`| xtp_kmc_run -o options.xml -f state.sql -e kmcmultiple`

### 2.9.1 Extrapolation to nondispersive mobilities

sec:nondispersive

Predictions of charge-carrier mobilities in partially disordered semiconductors rely on charge transport simulations in systems which are only several nanometers thick. As a result, simulated charge transport might be dispersive for materials with large energetic disorder [38, 39] and simulated mobilities are system-size dependent. In time-of-flight (TOF) experiments, however, a typical sample thickness is in the micrometer range and transport is often nondispersive. In order to link simulation and experiment, one needs to extract the nondispersive mobility from simulations of small systems, where charge transport is dispersive at room temperature.

Such extrapolation is possible if the temperature dependence of the nondispersive mobility is known in a wide temperature range. For example, one can use analytical results derived for one-dimensional models [40–42]. The mobility-temperature dependence can then be parametrized by



510 simulating charge transport at elevated temperatures, for which transport is nondispersive even  
 511 for small system sizes. This dependence can then be used to extrapolate to the nondispersive  
 512 mobility at room temperature [43].

513 For Alq<sub>3</sub>, the charge carrier mobility of a periodic system of 512 molecules was shown to be  
 514 more than three orders of magnitude higher than the nondispersive mobility of an infinitely  
 515 large system [43]. Furthermore, it was shown that the transition between the dispersive and  
 516 nondispersive transport has a logarithmic dependence on the number of hopping sites  $N$ . Hence,  
 517 a brute-force increase of the system size cannot resolve the problem for compounds with large  
 518 energetic disorder  $\sigma$ , since  $N$  increases exponentially with  $\sigma^2$ .

## 519 2.10 Stochastic Networks

sec:stochastic

520 The VOTCA package contains the functionality of generating large, amorphous charge transport  
 521 networks ( $\sim 10^6$  molecules). This is done with a combined coarse-grained and stochastic ap-  
 522 proach. VOTCA::CSG is used to generate a coarse-grained morphology. The stochastic modeling  
 523 of VOTCA::CTP allows to make a charge transfer network out of this morphology by reproduc-  
 524 ing the neighbor list (connectivity), transfer integrals, correlated site energies. An overview is  
 525 given in Figure 2.5.

526 Throughout this section we will use two state files. One is the state file `state_ref.sql` of the  
 527 smaller reference system that can be generated as explained in the previous sections. The second  
 528 one is the state file `state_cg.sql` of the coarse-grained system, or the stochastic network, that  
 529 can be parametrized as explained in this section.

530 When using the stochastic functionalities, please cite the corresponding work:

- 531 1. B. Baumeier, O. Stenzel, C. Poelking, D. Andrienko, and V. Schmidt: Stochastic modeling of  
 532 molecular charge transport networks. *Phys. Rev. B* 86, 184202 (2012)
- 533 2. P. Kordt and D. Andrienko: Modeling of Spatially Correlated Energetic Disorder in Organic  
 534 Semiconductors. *Journal of Chemical Theory and Computation* 12, 36–40 (2016)
- 535 3. P. Kordt, J. J. M. van der Holst, M. Al Helwi, W. Kowalsky, F. May, A. Badinski, C. Lennartz,  
 536 and D. Andrienko: Modeling of Organic Light Emitting Diodes: From Molecular to Device  
 537 Properties. *Advanced Functional Materials* 25, 1955–1971 (2015)

### 538 2.10.1 Coarse-grained morphology

539 The first step is to generate a coarse-grained morphology. In this example, it is done by mapping  
 540 a DPBIC molecule (which consists of 103 atoms) to a single point, its center of mass and by using  
 541 the iterative Boltzmann inversion (IBI) method. Starting point is a smaller reference morphology,  
 542 generated with GROMACS. Using the command

```
543 g_rdf -f traj.xtc -s topol.tpr
```

544 you can extract the radial distribution function  $g(r)$  of your reference topology, outputted into the  
 545 file `rdf.xvg`. This file, together with `table.xvg`, `grompp.mdp`, `topol.top`, `index.ndx` and `confout.gro`  
 546 form your reference data.

547 For VOTCA::CSG you need a `setting.xml` file:

```
548
549 <cg>
550   <!-- example for a non-bonded interaction entry -->
551   <non-bonded>
552     <!-- name of the interaction -->
553     <name>IR-IR</name>
554     <!-- types involved in this interaction -->
555     <type1>IR</type1>
556     <type2>IR</type2>
```



```

557 <!-- dimension + grid spacing of tables for calculations -->
558 <min>0.5</min>
559 <max>5.0</max>
560 <step>0.01</step>
561 <inverse>
562   <!-- target distribution (rdf), just give gromacs rdf.xvg -->
563   <target>rdf.xvg</target>
564   <!-- update cycles -->
565   <do_potential>1</do_potential>
566   <!-- additional post processing of dU before added to potential -->
567   <post_update>scale smooth</post_update>
568   <post_update_options>
569     <scale>0.5</scale> <!--Scale the potential before updating it -->
570     <smooth>
571       <iterations>2</iterations>
572     </smooth>
573   </post_update_options>
574   <!-- additional post processing of U after dU added to potential -->
575   <post_add></post_add>
576   <!-- name of the table for gromacs run -->
577   <gromacs>
578     <table>table_IR_IR.xvg</table>
579   </gromacs>
580 </inverse>
581 </non-bonded>
582
583 <!-- general options for inverse script -->
584 <inverse>
585   <!-- 300*0.00831451 gromacs units -->
586   <kBT>2.49435300</kBT>
587   <initial_configuration>maindir</initial_configuration>
588   <!-- use gromacs as simulation program -->
589   <program>gromacs</program>
590   <!-- gromacs specific options -->
591   <gromacs>
592     <!-- trash so many frames at the beginning -->
593     <equi_time>500</equi_time>
594     <!-- grid for table*.xvg !-->
595     <table_bins>0.001</table_bins>
596     <!-- cut the potential at this value (gromacs bug) -->
597     <pot_max>1000000</pot_max>
598     <!-- extend the tables to this value -->
599     <table_end>6.0</table_end>
600   </gromacs>
601   <!-- these files are copied for each new run -->
602   <filelist>grompp.mdp topol.top index.ndx table.xvg</filelist>
603   <!-- do so many iterations -->
604   <iterations_max>500</iterations_max>
605   <!-- Try to clean a bit -->
606   <cleanlist>traj.xtc</cleanlist>
607   <!-- ibm: inverse boltzmann imc: inverse monte carlo -->
608   <method>ibi</method>
609   <!-- write log to this file -->
610   <log_file>inverse.log</log_file>
611   <!-- write restart step to this file -->
612   <restart_file>restart_points.log</restart_file>
613   <!-- imc specific stuff -->
614 </inverse>

```

---

```
</cg>
```

---

You run IBI using the command

```
csg_inverse -options settings.xml
```

IBI intends to find a potential  $U(r)$  that reproduces your radial distribution function. It is stored in the file **table\_IR\_IR.xvg** in our example.

With the interaction potential at hand, a large topology can be generated using molecular dynamics simulations for the coarse grained model. Starting point is a box with equally distributed points, with each point representing one molecule and with the number of points chosen such that the density of the reference system is reproduced. A small python script can generate the conf.gro to start from, here shown to obtain a  $50 \times 50 \times 120 \text{ nm}^3$  starting morphology.

```
from pylab import *
import numpy as np

lenX      = 50
lenY      = 50
lenZ      = 120
originalV = 4704.339
originalN = 4000
spacing   = (originalV/originalN)**(1./3.)

molecule = "DPBIC"
resname   = "IRI"
atomname  = "IR"

newV = lenX*lenY*lenZ
newN = int(newV/originalV*originalN)

nX = int(lenX/spacing)+1
nY = int(lenY/spacing)+1
nZ = int(lenZ/spacing)+1

print "max. molecules in X direction: "+str(nX)
print "max. molecules in Y direction: "+str(nY)
print "max. molecules in Z direction: "+str(nZ)
print "total number of molecules: "+str(newN)

file = open("box.gro", "w")
file.write(molecule+"\n")
file.write(str(newN)+"\n")

atomnumber = 1
for iX in range(nX):
    for iY in range(nY):
        for iZ in range(nZ):
            if(atomnumber > newN):
                break
            posX = spacing*iX
            posY = spacing*iY
            posZ = spacing*iZ
            print ">> file, \"%5d%-5s%5s%5d%8.3f%8.3f%8.3f%8.4f%8.4f%8.4f\" % \\"
                  (1,resname,atomname,1,posX,posY,posZ,0,0,0)
            atomnumber += 1

file.write(" "+str(lenX)+" "+str(lenY)+" "+str(lenZ))
```

```

673 file.close()
674
675 print "Note: for some obscure reason VMD will not be able to read this file\
676 properly unless you open it once in vi and save it."
677

```

678 Open the `box.gro` in `vi` and save it (`:wq`), afterwards you can have a look at it in VDM. Run your  
 679 MD simulations using the `mdrun` command. In the end you can compare the radial distribution  
 680 functions of your reference and coarse-grained system, as shown in figure 2.6(a) as an example.

## 681 2.10.2 Charge transport network

682 To generate a charge transport network you first need a reference system with neighbor list, site  
 683 energies and transfer integrals calculated and stored in a **state.sql** state file. The procedure for all  
 684 these three properties is always the same: first analyze the reference data, and second import the  
 685 analyzation files and reproduce the properties.

### 686 Neighbor list

687 In the atomistic reference system molecules are connected if their two closest segments are below  
 688 a certain cut-off radius. This finer picture of segments does not exist in the coarse-grained system,  
 689 where each molecule is represented by a point. To mimick the neighbor list, the probability of  
 690 two molecules to be connected is analyzed as a function of their center-of-mass distance. This  
 691 can be done by using the *panalyze* calculator

 **Analyze the pair connectivity (neighborlist) in the reference system**  
 | `xtp_run -o options.xml -f state_ref.sql -e panalyze`

692 with the options defined as follows:

#### 693 options\_analyze.xml

```

694 <options>
695   <panalyze>
696     <resolution_space>0.05</resolution_space>
697   </panalyze>
698 </options>
699

```

702 The only parameter needed is the spacial resolution, i.e., the bin size for calculating the probabil-  
 703 ities. The *panalyze* calculator outputs a file **panalyze.distanceprobability.out** with the respective  
 704 probabilities. Now this file has to be imported into the coarse-grained state file

 **Import the reference pair connectivity (neighborlist) and reproduce it in stochastic network**  
 | `xtp_run -o options.xml -f state_cg.sql -e neighborlist`

705 using the following options:

#### 706 options\_import.xml

```

707 <options>
708   <neighborlist>
709     <probabilityfile>panalyze.distanceprobability.out</probabilityfile>
710   </neighborlist>
711 </options>
712

```

715 For testing purposes, you can run the *panalyze* calculator on your coarse-grained state file and  
 716 compare the probability function to the reference. An example is shown in figure 2.6(b). You  
 717 can also also look at the file **panalyze.distanceprobability.out** for both state files, which has the  
 718 distribution of coordination numbers (number of neighbors) and its average in.

## Site energies

Site energies in amorphous organic semiconductors are roughly Gaussian distributed, with the width of the Gaussian,  $\sigma$ , called the energetic disorder. However, there are correlations between sites if they are close enough to each other. The aim in this section is therefore to reproduce the correlated energetic landscape. The first step is to get a spatial correlation function as well as the mean energy and the energetic disorder from your reference state file:

 **Analyze the energy distribution and correlation in the reference system**  
 | `xtp_run -o options.xml -f state_ref.sql -e eanalyze`

with the following options:

### options\_analyze.xml

```
<options>
  <eanalyze>
    <resolution_sites>0.05</resolution_sites>
    <resolution_pairs>0.05</resolution_pairs>
    <resolution_space>0.3</resolution_space>
    <states>1,-1</states> <!-- +1 for hole transport, -1 for electron transport -->
    <distancemode>centreofmass</distancemode>
  </eanalyze>
</options>
```

The first three parameters determine bin sizes, then you can choose to look at hole and/or electron energy. The keyword *centreofmass* means, that the correlation function is calculated as a function of the centre-of-mass distance of molecules and not as a function of their nearest segments. For the stochastic simulations you always have to use the *centreofmass* mode!

The output files of this calculator that we need are **eanalyze.sitecorr\_e.out** (for electrons) and **eanalyze.sitecorr\_h.out** (for holes). In the second line of this file, you find mean and sigma of the energy distribution, as well as the mean of the static energies (without induction):

```
# EANALYZE: SPATIAL SITE-ENERGY CORRELATION
# AVG -0.4412655 STD 0.1739638 MIN_R 0.8365040 MAX_R 14.4771496 AVGESTATIC
-0.4730655
...
```

These values have to be inserted manually into the options file for importing to the coarse-grained system (see below). Apart from that, the file contains the spatial correlation function.

You generate energies following this distribution and correlation by using the *eimport* calculator

 **Import the energy distribution and correlation and reproduce it in stochastic network**  
 | `xtp_run -o options.xml -f state_ref.sql -e eimport`

with the options:

### options\_import.xml

```
<options>
  <eimport>
    <probabilityfile_h>reference/eanalyze.sitecorr_h.out</probabilityfile_h>
    <sigma_h>0.1763163</sigma_h>
    <avgestatic_h>-0.5913265</avgestatic_h>
    <probabilityfile_e>reference/eanalyze.sitecorr_e.out</probabilityfile_e>
```

```

766         <sigma_e>0.1739638</sigma_e>
767         <avgestatic_e>-0.4730655</avgestatic_e>
768         <cutoff>8.5</cutoff>
769         <seed>1</seed>
770     </eimport>
771 </options>
772

```

773 The *cutoff* keyword can be used to read in the correlation function only up to a certain distance, which can be useful if larger distances yield unphysical results.

## 775 Transfer Integrals

776 The last ingredient reproduced by the stochastic approach are transfer integrals  $J$ . The idea is that  $\log_{10}(J^2/\text{eV}^2)$  is roughly Gaussian distributed, with mean and error of the distribution varying with distance (see figure 2.6 (d)). Use the calculator

779

 **Analyze the distance-depend distribution of transfer integrals in the reference system**  
**|** `xtp_run -o options.xml -f state_ref.sql -e ianalyze`

780 with options

781

## 782 options\_analyze.xml

```

783 <options>
784     <ianalyze>
785         <resolution_logJ2>0.05</resolution_logJ2>
786         <resolution_space>0.05</resolution_space>
787         <states>1,-1</states> <!-- +1 for hole transport, -1 for electron transport -->
788     </ianalyze>
789 </options>
790
791

```

792 That will generate the files **ianalyze.ispatial\_e.out** and **ianalyze.ispatial\_h.out**, which contain means and errors as a function of centre-of-mass distance.

794

795 Now use the *iimport* calculator to generate transfer integrals in the coarse grained state file, following the same statistics.

796

 **Import distance dependent distribution of transfer integrals and reproduce in stochastic network**  
**|** `xtp_run -o options.xml -f state_cg.sql -e iimport`

## 797 options\_import.xml

```

798 <options>
799     <iimport>
800         <TI_tag></TI_tag>
801         <TI_file></TI_file>
802         <idft_jobs_file></idft_jobs_file>
803         <probabilityfile_h>reference/ianalyze.ispatial_h.out</probabilityfile_h>
804         <probabilityfile_e>reference/ianalyze.ispatial_e.out</probabilityfile_e>
805     </iimport>
806 </options>
807
808

```

## 809 einternal

810 Run the *einternal* calculator, just as you do it for the reference system.

## Rates

If you followed the steps in this section, you have everything at hand to calculate charge transfer rates for the coarse grained system from the stochastic ingredients:



### Calculate rates in the stochastic network

```
xtp_run -o options.xml -f state_cg.sql -e rates
```

Options are the same as for the reference file. You can check the result by comparing rates from your reference to the coarse-grained system, see figure 2.6(e) for an example. The resulting charge transport network can be used for kinetic Monte Carlo simulations with VOTCA. If everything goes well, mobilities for both systems should agree, as shown in figure 2.6(f).

## 2.11 Macroscopic observables

sec:analysis

Spatial distributions of charge and current densities can provide a better insight in the microscopic mechanisms of charge transport. If  $O$  is an observable which has a value  $O_\alpha$  in a state  $\alpha$ , its ensemble average at time  $t$  is a sum over all states weighted by the probability  $P_\alpha$  to be in a state  $\alpha$  at time  $t$

$$\langle O \rangle = \sum_{\alpha} O_{\alpha} P_{\alpha}. \quad (2.36) \quad \text{equ:ensemble}$$

If  $O$  does not explicitly depend on time, the time evolution of  $\langle O \rangle$  can be calculated as

$$\frac{d\langle O \rangle}{dt} = \sum_{\alpha, \beta} [P_{\beta} \Omega_{\beta\alpha} - P_{\alpha} \Omega_{\alpha\beta}] O_{\alpha} = \sum_{\alpha, \beta} P_{\beta} \Omega_{\beta\alpha} [O_{\alpha} - O_{\beta}]. \quad (2.37)$$

If averages are obtained from KMC trajectories,  $P_{\alpha} = s_{\alpha}/s$ , where  $s_{\alpha}$  is the number of Markov chains ending in the state  $\alpha$  after time  $t$ , and  $s$  is the total number of chains.

Alternatively, one can calculate time averages by analyzing a single Markov chain. If the total occupation time of the state  $\alpha$  is  $\tau_{\alpha}$  then

$$\overline{O} = \frac{1}{\tau} \sum_{\alpha} O_{\alpha} \tau_{\alpha}, \quad (2.38) \quad \text{equ:time}$$

where  $\tau = \sum_{\alpha} \tau_{\alpha}$  is the total time used for time averaging.

For ergodic systems and sufficient sampling times, ensemble and time averages should give identical results. In many cases, the averaging procedure reflects a specific experimental technique. For example, an ensemble average over several KMC trajectories with different starting conditions corresponds to averaging over injected charge carriers in a time-of-flight experiment. In what follows, we focus on the single charge carrier (low concentration of charges) case.

### 2.11.1 Charge density

sec:occupation

For a specific type of particles, the microscopic charge density of a site  $i$  is proportional to the occupation probability of the site,  $p_i$

$$\rho_i = e p_i / V_i, \quad (2.39)$$

where, for an irregular lattice, the effective volume  $V_i$  can be obtained from a Voronoi tessellation of space. For reasonably uniform lattices (uniform site densities) this volume is almost independent of the site and a constant volume per site,  $V_i = V/N$ , can be assumed. In the macroscopic limit, the charge density can be calculated using a sxtpting kernel function, i.e. a distance-weighted average over multiple sites. Site occupations  $p_i$  can be obtained from eq. (2.36) or eq. (2.38) by using the occupation of site  $i$  in state  $\alpha$  as an observable.

If the system is in thermodynamic equilibrium, that is without sources or sinks and without circular currents (and therefore no net flux) a condition, known as detailed balance, holds

$$p_j \omega_{ji} = p_i \omega_{ij}, \quad (2.40) \quad \text{equ:detailed\_balance}$$

It can be used to test whether the system is ergodic or not by correlating  $\log p_i$  and the site energy  $E_i$ . Indeed, if  $\lambda_{ij} = \lambda_{ji}$  the ratios of forward and backward rates are determined solely by the energetic disorder,  $\omega_{ji}/\omega_{ij} = \exp(-\Delta E_{ij}/k_B T)$  (see eq. (2.31)).

### 2.11.2 Current

If the position of the charge,  $\vec{r}$ , is an observable, the time evolution of its average  $\langle \vec{r} \rangle$  is the total current in the system

$$\vec{J} = e \langle \vec{v} \rangle = e \frac{d \langle \vec{r} \rangle}{dt} = e \sum_{i,j} p_j \omega_{ji} (\vec{r}_i - \vec{r}_j). \quad (2.41) \quad \text{equ:current\_def}$$

Symmetrizing this expression we obtain

$$\vec{J} = \frac{1}{2} e \sum_{i,j} (p_j \omega_{ji} - p_i \omega_{ij}) \vec{r}_{ij}, \quad (2.42) \quad \text{equ:current}$$

where  $\vec{r}_{ij} = \vec{r}_i - \vec{r}_j$ . Symmetrization ensures equal flux splitting between neighboring sites and absence of local average fluxes in equilibrium. It allows to define a local current through site  $i$  as

$$\vec{J}_i = \frac{1}{2} e \sum_j (p_j \omega_{ji} - p_i \omega_{ij}) \vec{r}_{ij}. \quad (2.43) \quad \text{equ:site\_current}$$

A large value of the local current indicates that the site contributes considerably to the total current. A collection of such sites thus represents most favorable charge pathways [44].

### 2.11.3 Mobility and diffusion constant

For a single particle, e.g. a charge or an exciton, a zero-field mobility can be determined by studying particle diffusion in the absence of external fields. Using the particle displacement squared,  $\Delta \mathbf{r}_i^2$ , as an observable we obtain

$$2dD_{\gamma\delta} = \frac{d \langle \Delta r_{i,\gamma} \Delta r_{i,\delta} \rangle}{dt} = \sum_{\substack{i,j \\ i \neq j}} p_j \omega_{ji} (\Delta r_{i,\gamma} \Delta r_{i,\delta} - \Delta r_{j,\gamma} \Delta r_{j,\delta}) = \sum_{\substack{i,j \\ i \neq j}} p_j \omega_{ji} (r_{i,\gamma} r_{i,\delta} - r_{j,\gamma} r_{j,\delta}). \quad (2.44) \quad \text{equ:diffusion}$$

Here  $\vec{r}_i$  is the coordinate of the site  $i$ ,  $D_{\gamma\delta}$  is the diffusion tensor,  $\gamma, \delta = x, y, z$ , and  $d = 3$  is the system dimension. Using the Einstein relation,

$$D_{\gamma\delta} = k_B T \mu_{\gamma\delta}, \quad (2.45)$$

one can, in principle, obtain the zero-field mobility tensor  $\mu_{\gamma\delta}$ . Eq. (2.44), however, does not take into account the use of periodic boundary conditions when simulating charge dynamics. In this case, the simulated occupation probabilities can be compared to the solution of the Smoluchowski equation with periodic boundary conditions (see the supporting information for details).

Alternatively, one can directly analyze time-evolution of the KMC trajectory and obtain the diffusion tensor from a linear fit to the mean square displacement,  $\overline{\Delta r_{i,\gamma} \Delta r_{i,\delta}} = 2dD_{\gamma\delta}t$ .

The charge carrier mobility tensor,  $\hat{\mu}$ , for any value of the external field can be determined either from the average charge velocity defined in eq. (2.41)

$$\langle \vec{v} \rangle = \sum_{i,j} p_j \omega_{ji} (\vec{r}_i - \vec{r}_j) = \hat{\mu} \vec{F}, \quad (2.46)$$

or directly from the KMC trajectory. In the latter case the velocity is calculated from the unwrapped (if periodic boundary conditions are used) charge displacement vector divided by the total simulation time. Projecting this velocity on the direction of the field  $\vec{F}$  yields the charge carrier mobility in this particular direction. In order to improve statistics, mobilities can be averaged over several KMC trajectories and MD snapshots.

#### 2.11.4 Spatial correlations of energetic disorder

Long-range, e.g. electrostatic and polarization, interactions often result in spatially correlated disorder [45], which affects the onset of the mobility-field (Poole-Frenkel) dependence [40, 46, 47]. To quantify the degree of correlation, one can calculate the spatial correlation function of  $E_i$  and  $E_j$  at a distance  $r_{ij}$

$$C(r_{ij}) = \frac{\langle (E_i - \langle E \rangle) (E_j - \langle E \rangle) \rangle}{\langle (E_i - \langle E \rangle)^2 \rangle}, \quad (2.47)$$

where  $\langle E \rangle$  is the average site energy.  $C(r_{ij})$  is zero if  $E_i$  and  $E_j$  are uncorrelated and 1 if they are fully correlated. For a system of randomly oriented point dipoles, the correlation function decays as  $1/r$  at large distances [48].

For systems with spatial correlations, variations in site energy differences,  $\Delta E_{ij}$ , of pairs of molecules from the neighbor list are smaller than variations in site energies,  $E_i$ , of all individual molecules. Since only neighbor list pairs affect transport, the distribution of  $\Delta E_{ij}$  rather than that of individual site energies,  $E_i$ , should be used to characterize energetic disorder.

Note that the `eanalyze` calculator takes into account *all* contributions to the site energies

 **Analyze distribution and correlations of site energieis**  
`| xtp_run -o options.xml -f state.sql -e eanalyze`

## 2.12 Random Facts

This section is a collection of facts we discovered about xtp and ctp which should be included in the manual at some point, but lack proper background.

### 2.12.1 xqmm

The cutoffs used should not exceed the dimension of the cell, at least for a non orthogonal unit cell. XQMM throws an error if your cutoff is larger than the box, but it does not take the extension of the molecule into account, so often you may still have overlap.

XQMMM takes the segment coordinates from the MPS\_Files so be vary careful which MPS\_File you put in.

### 2.12.2 EWALD

- Use `pewald3d`, as a calculator. I am not sure what the rest is for. All still use the ewald options. The shape factor massively influences the results. For bulk systems "none" is the option of choice. Other options are "xyslab", "sphere", "cube" but I do not know what they do.
- The induction cutoff should hardly ever exceed 3nm, because the calculation is expensive
- If you want to use induction, you before have to run `ewdbgp` calculator and specify `polar_top.bgp` in the options file for ewald. All the other parameters should be the same in `ewdbgp` and `pewald3d`



### 2.12.3 GW-BSE

There is a wide range of different approximations for *GW*-BSE. Here I try to summarize common abbreviations and methods and explain what our code does. This is not complete and certainly has some mistakes in it.

- COHSEX: RPA is only calculated for  $\omega = 0$ . This amounts to  $\varepsilon(\bar{\mathbf{r}}, \bar{\mathbf{r}}', \omega) = \varepsilon(\bar{\mathbf{r}}, \bar{\mathbf{r}}')$ . This is also called the static approximation to *GW*
- Plasmon Pole model; RPA is calculated mostly twice, once at  $\omega = 0$  and  $\omega = \omega_0$ , then these values are used to fit an analytic model to interpolate  $\varepsilon(\bar{\mathbf{r}}, \bar{\mathbf{r}}', \omega)$ .
- Imaginary frequency integration,  $\varepsilon$  is numerically integrated along the Imaginary frequency axis. This is done because  $\varepsilon$  is much smoother along the Imaginary axis and thus requires less functional evaluations. Afterwards  $\varepsilon$  is extended to real frequencies via analytic continuation.

The calculation of *GW*. In VOTCA we also have the **shift** option. This is commonly called a scissor operator. This allows you to shift the unoccupied KS-orbitals up in energy, making the resulting spectrum closer to the *GW* spectrum. This is often a better starting point for the self-consistent evaluations.

- $G_0W_0$ .  $G$  and  $\varepsilon$  are calculated once from DFT results.  $W$  is evaluated once from that. Then energies  $\varepsilon_i^{GW}$  are corrected via:

$$\varepsilon_i^{GW} = \varepsilon_i^{KS} + Z_i \langle \phi_i^{KS} | \Sigma(\varepsilon_i^{KS}) - V_{xc} | \phi_i^{KS} \rangle \quad (2.48)$$

This is not implemented in VOTCA, because  $GW_0$  is nearly as fast.

- $GW_0$ .  $\varepsilon$  is calculated once from DFT results.  $W$  is evaluated once from that. Then  $\Sigma$  is calculated. The resulting energies are fed back into  $\Sigma$ , until self-consistency is achieved. This is denoted **fixed** in VOTCA.

$$\varepsilon_i^{GW} = \varepsilon_i^{KS} + \langle \phi_i^{KS} | \Sigma(\varepsilon_i^{GW}) - V_{xc} | \phi_i^{KS} \rangle \quad (2.49)$$

- *scQPGW*. As  $GW_0$ , but after  $\varepsilon_i^{GW}$  are converged, these energies are used to recalculate  $\varepsilon$  and then  $W$ , this is repeated until self-consistency is achieved. This is denoted **iterate** in VOTCA. This converges the “eigenvalues” of QP particles but along the  $|\phi^{GW}\rangle$  states
- *scGW*. As *scQPGW* but instead of correcting only the energies, the full *Sigma* matrix is calculated and the eigenvalue problem for the QP is set up and solved and the whole system is then self-consistently solved in  $|\phi^{GW}\rangle$  states and not in  $|\phi^{KS}\rangle$ . This fully converges the eigenvalues and eigenvectors of the QP particles in the space spanned by  $|\phi^{KS}\rangle$ , e.g.  $|\phi^{GW}\rangle$  are linear combinations of  $|\phi^{KS}\rangle$ . This is reported to be unstable because the vertex corrections are important now. This is at the moment implemented in VOTCA.

The calculations in BSE

-

MORPHOLOGY		
	EXTRACT	REPRODUCE
<b>RDF and coarse grained potential</b>	GROMACS <code>g_rdf -f traj.xtc -s topol.tpr</code>	VOTCA::CSG <code>csg_inverse -options settings.xml</code>
<b>morphology</b>		GROMACS <code>mdrun</code>

RATES		
	EXTRACT	REPRODUCE
<b>neighbor list (pairs)</b>	<code>xtp_run -e panalyze -o options.xml -f state_reference.sql</code>	<code>xtp_run -e neighborlist -o options.xml -f state_cg.sql</code>
<b>site energies</b>	<code>xtp_run -e eanalyze -o options.xml -f state_reference.sql</code>	<code>xtp_run -e eimport -o options.xml -f state_cg.sql</code>
<b>transfer integrals</b>	<code>xtp_run -e ianalyze -o options.xml -f state_reference.sql</code>	<code>xtp_run -e iimport -o options.xml -f state_cg.sql</code>
<b>rates</b>	not used directly	<code>xtp_run -e rates -o options.xml -f state_cg.sql</code>

Figure 2.5: Stochastic Model in VOTCA. Overview of the different steps for generating stochastic charge transport networks in VOTCA. The Molecular Dynamics software GROMACS allows to analyze the radial distribution function of a morphology, which is then used by VOTCA::CSG to generate a coarse-grained potential that reproduces this distribution function. This potential can then be used for coarse-grained simulations in GROMACS. For calculating rates in the coarse-grained morphology, first the relevant parameters are extracted (panalyze, eanalyze, ianalyze) from the reference morphology and then reproduced in the coarse-grained morphology (neighborlist, eimport, iimport). With all these at hand, the rates calculator can be used in the coarse-grained morphology.



Figure 2.6: Comparison of the atomistic ( $17 \times 17 \times 17$  nm<sup>3</sup>) and coarse-grained ( $50 \times 50 \times 120$  nm<sup>3</sup>) models. (a) Radial distribution function,  $g(r)$ . (b) Probability of two sites to be connected (added to the neighbor list) as a function of their separation. (c) Spatial site energy autocorrelation function,  $\kappa(r)$ ; Inset: Site energy distribution. (d) Mean  $m$  and width  $\sigma$  of a distribution of the logarithm of electronic couplings,  $\log_{10}(J^2/eV^2)$ , for molecules at a fixed separation  $r$ . (e) Rate distributions. (f) Mobility as a function of hole density, plotted for four different electric fields.

fig:stochastic



## Chapter 3

# Input and output files

### 3.1 Atomistic topology

If you are using GROMACS for generating atomistic configurations, it is possible to directly use the topology file provided by GROMACS (`topology.tpr`). In this case the GROMACS residue and atom names should be used to specify the coarse-grained topology and conjugated segments. A custom topology can also be defined using an XML file. Moreover, it is possible to partially overwrite the information provided in, for example, GROMACS topology file. We will illustrate how to create a custom topology file using DCV2T. The structure of DCV2T, together with atom type definitions, is shown in fig. 3.1. DCV2T has two thiophene (THI) and two dicyanovinyl (NIT) residues. The pdb file which contains residue types, residue numbering, atom names, atom types, and atom coordinates is shown in listing 3.1.



Figure 3.1: (a) DCV2T with atoms labelled according to `residue_number:residue_name:atom_name`. There are four residues and two residue types: thiophene (THI) and dicyanovinyl (NIT). The corresponding pdb file is shown in listing 3.1. Atom numbering is used to split conjugated segments on rigid fragments and to link atomistic ((b) from GROMACS topology) and quantum descriptions (c).

fig:dcv2t

list:pdb

Listing 3.1: pdb file of DCV2T.

949	HETATM	1	N1	NIT	1	2.388	8.533	11.066	1.00	4.14	N
950	HETATM	2	CN1	NIT	1	1.984	9.553	10.718	1.00	2.54	C
952	HETATM	3	N2	NIT	1	-1.138	10.872	10.087	1.00	3.24	N
953	HETATM	4	CN2	NIT	1	0.003	10.871	10.213	1.00	2.37	C
954	HETATM	5	CC1	NIT	1	1.441	10.824	10.327	1.00	1.91	C
955	HETATM	6	C1	NIT	1	2.193	11.939	10.071	1.00	1.61	C
956	HETATM	7	HN1	NIT	1	1.715	12.710	9.872	1.00	1.97	H
957	HETATM	8	S1	THI	2	4.758	10.743	10.130	1.00	1.52	S
958	HETATM	9	CA1	THI	2	3.613	12.024	9.948	1.00	1.22	C
959	HETATM	10	CA2	THI	2	6.099	11.836	9.997	1.00	1.30	C
960	HETATM	11	CB1	THI	2	4.251	13.243	9.782	1.00	1.39	C
961	HETATM	12	CB2	THI	2	5.658	13.131	9.818	1.00	1.45	C
962	HETATM	13	HC1	THI	2	3.800	14.047	9.660	1.00	1.66	H
963	HETATM	14	HC2	THI	2	6.230	13.860	9.731	1.00	1.74	H
964	HETATM	15	S1	THI	3	8.803	12.414	9.882	1.00	1.38	S
965	HETATM	16	CA1	THI	3	7.456	11.347	10.094	1.00	1.37	C
966	HETATM	17	CA2	THI	3	9.940	11.122	10.152	1.00	1.42	C
967	HETATM	18	CB1	THI	3	7.873	10.048	10.355	1.00	1.73	C
968	HETATM	19	CB2	THI	3	9.267	9.926	10.399	1.00	1.82	C
969	HETATM	20	HC1	THI	3	7.288	9.335	10.487	1.00	2.05	H
970	HETATM	21	HC2	THI	3	9.704	9.123	10.576	1.00	2.21	H
971	HETATM	22	N1	NIT	4	11.235	14.572	9.094	1.00	3.08	N
972	HETATM	23	CN1	NIT	4	11.665	13.566	9.441	1.00	2.04	C
973	HETATM	24	N2	NIT	4	14.733	12.005	10.009	1.00	2.17	N
974	HETATM	25	CN2	NIT	4	13.590	12.149	9.933	1.00	1.77	C
975	HETATM	26	CC1	NIT	4	12.156	12.282	9.861	1.00	1.71	C
976	HETATM	27	C1	NIT	4	11.363	11.220	10.154	1.00	1.59	C
977	HETATM	28	HN1	NIT	4	11.813	10.440	10.389	1.00	1.89	H

tab:map

Table 3.1: Description of the XML mapping file (`map.xml`).

topology	Definitions of molecules, segments, and fragments.
molecules	Container for all molecules.
molecule	Mapping of a single molecule.
name	Name of the molecule in the coarse-grained model.
ident	Name (identification) of the molecule in the all-atom representation. This must match the molecule name in the atomistic representation.
segments	Partitioning of the molecule on conjugated segments.
segment	Description of a conjugated segment.
name	Name of a conjugated segment in a molecule.
fragments	Container for all fragments in a segment.
fragment	Description of a rigid fragment.
name	Name of the rigid fragment in a conjugated segment
mdatoms	List of all atoms belonging to the rigid fragment in the format residue number:residue name:atom name.
qmatoms	List of atoms of the rigid fragment in its ground state geometry, atom number:atom type.
weights	Weights are used to determine the fragment center. The order should be the same as in the mdatoms and qmatoms definitions. If the mass of a nucleus in atomic mass units is used, the center of the rigid fragment will be its center of mass.
localframe	Three atoms which define a local frame for each rigid fragment.

## 3.2 Mapping file

979

sec:xmlmap

980

981

982

983

984

985

986

987

988

989

990

991

992

993

994

995

996

997

998

999

1000

1001

1002

1003

1004

1005

1006

1007

1008

1009

1010

1011

1012

1013

1014

1015

The mapping file (referred here as `map.xml`) is used by the program `xtp_map` to convert an atomistic trajectory to a trajectory with conjugated segments and rigid fragments. This trajectory is stored in a state file and contains positions, names, types of atoms belonging to rigid fragments. The description of the mapping options is given in table 3.1. An example of `map.xml` for a DCV2T molecule is shown in listing 3.2.

The file `map.xml` contains the whole electrostatic information about the molecules as well as the structural information. The `toolpdb2map` creates a `map.xml` from a `pdb` file and is a good starting point for further refinement.

list:map

Listing 3.2: Examl of `map.xml` for DCV2T. Each rigid fragment (coarse-grained bead) is defined by a list of atoms. Atom numbers, names, and residue names should correspond to those used in GROMACS topology (see the corresponding listing 3.1 of the `pdb` file).

```

988 <!-- this file is used to conver an atomistic trajectory to conjugated segments -->
989 <!-- molecules -->
990 <!-- molecule -->
991 <!-- name of the conjugated molecule -->
992 <!-- corresponding name of this molecule in the MD trajectory, should be
993 the same as the name given at the end of topol.top -->
994 <!-- segments -->
995 <!-- segment -->
996 <!-- name of the conjugated segment within the molecule -->
997 <!-- QM coordinates of the conjugated segment -->
998
999
1000
1001 <!-- IZINDO INPUT -->
1002 <!-- basisset -->
1003 <!-- orbitals -->
1004 <!-- Number of the HOMO Orbital (e.g. alpha electrons, can be
1005 found in the log-file belonging to DCV2T.orb) -->
1006
1007 <!-- EMULTIPOLE INPUT -->
1008 <!-- Multipole file for neutral state -->
1009 <!-- Multipole file for hole state -->
1010
1011 <!-- specifies if planar QM coordinates (map2md=0) or MD coordinates (
1012 map2md=1) of atoms are used for distribution of partial charges. For MD coordinates the
1013 order and numbering in <mdatoms> and <mipoles> must be identical it has no impact on the
1014 qm e.g. DFT or GWBSE calculations -->
1015

```

```

1016 <!-- EINTERNAL INPUT -->
1017 <U_cN_nN_h>0.0</U_cN_nN_h> <!-- Site energy -->
1018 <U_nC_nN_h>0.1</U_nC_nN_h> <!-- Reorg. discharge -->
1019 <U_cN_cC_h>0.1</U_cN_cC_h> <!-- Reorg. charge -->
1020
1021 <!-- MD QM MP Mapping -->
1022 <fragments>
1023 <fragment>
1024 <name>NI1</name> <!-- name of the rigid fragment within the segment -->
1025 <!-- list of atoms in the fragment resnum:resname:atomname -->
1026 <mdatoms>1:NIT:N1 1:NIT:CN1 1:NIT:N2 1:NIT:CN2 1:NIT:CC1 1:NIT:C1 1:NIT:HN1</mdatoms>
1027 <!-- corresponding ground state geometry atomnumber:atomtype read from .xyz file -->
1028 <qmatoms> 20:N 19:C 14:N 13:C 12:C 11:C 23:H </qmatoms>
1029 <!-- corresponding group state geometry multipoles read from .mps files -->
1030 <mpoles> 20:N 19:C 14:N 13:C 12:C 11:C 23:H </mpoles>
1031 <!-- weights to determine the fragment center (here CoM is used) -->
1032 <weights> 14 12 14 12 12 12 1 </weights>
1033 <!-- three atoms: define a cartesian local frame, two atoms: fragment is assumed to be
1034 rotationally invariant around the axis, one atom: fragment is assumed isotropic -->
1035 <localframe> 20 19 14 </localframe>
1036 <!-- Optional parameters (if not set <localframe> is used): used when atom labels in the .mps
1037 and .xyz file differ or more sites in the .mps file are used, so refers to <mpoles> -->
1038 <localframe_mps> 20 19 14 </localframe_mps>
1039 <!-- Optional parameters (if not set <localframe> is used): weights to determine the
1040 fragment center (here CoM is used), used when atom labels in the .mps and .xyz file
1041 differ or additional sites in the .mps file are used -->
1042 <weights_mps> 14 12 14 12 12 12 1 </
1043 weights_mps>
1044 <!-- Optional flag: says if a site is virtual or not, (virtual=1, real=0)-->
1045 <virtual_mps> 0 0 0 0 0 0 0 </
1046 virtual_mps>
1047 </fragment>
1048
1049 <fragment>
1050 <name>TH1</name>
1051 <mdatoms>2:THI:S1 2:THI:CA1 2:THI:CA2 2:THI:CB1 2:THI:CB2 2:THI:HC1 2:THI:HC2</mdatoms>
1052 <qmatoms> 7:S 8:C 6:C 9:C 10:C 24:H 25:H </qmatoms>
1053 <mpoles> 7:S 8:C 6:C 9:C 10:C 24:H 25:H </mpoles>
1054 <weights> 32 12 12 12 12 1 1 </weights>
1055 <localframe> 7 8 6 </localframe>
1056 </fragment>
1057
1058 <fragment>
1059 <name>TH2</name>
1060 <mdatoms>3:THI:S1 3:THI:CA1 3:THI:CA2 3:THI:CB1 3:THI:CB2 3:THI:HC1 3:THI:HC2</mdatoms>
1061 <qmatoms> 3:S 4:C 2:C 5:C 1:C 26:H 27:H </qmatoms>
1062 <weights> 32 12 12 12 12 1 1 </weights>
1063 <localframe> 3 4 2 </localframe>
1064 </fragment>
1065
1066 <fragment>
1067 <name>NI2</name>
1068 <mdatoms>4:NIT:N1 4:NIT:CN1 4:NIT:N2 4:NIT:CN2 4:NIT:CC1 4:NIT:C1 4:NIT:HN1</mdatoms>
1069 <qmatoms> 22:N 21:C 18:N 17:C 16:C 15:C 28:H </qmatoms>
1070 <mpoles> 22:N 21:C 18:N 17:C 16:C 15:C 28:H </mpoles>
1071 <weights> 14 12 14 12 12 12 1 </weights>
1072 <localframe> 22 21 18 </localframe>
1073 </fragment>
1074 </fragments>
1075 </segment>
1076 </segments>
1077 </molecule>
1078 </molecules>
1079 </topology>

```

### 3.3 Molecular orbitals

If the semi-empirical method is used to calculate electronic coupling elements, molecular orbitals of all molecules must be supplied. They can be generated using Gaussian program. The Gaussian input file for DCV2T is shown in listing 3.3. Provided with this input, Gaussian will generate fort.7 file which contains the molecular orbitals of a DCV2T. This file can be renamed to DCV2T.orb. Note that the order of the atoms in the input file and the order of coefficients should always match. Therefore, the coordinate part of the input file must be supplied together



1088 with the orbitals. We will assume the coordinates, in the format `atom_type: x y z`, is saved  
1089 to the `DCV2T.xyz` file.



#### Be careful!

Izindo requires the specification of orbitals for hole and electron transport in `map.xml`. They are the HOMO and LUMO respectively and can be retrieved from the `log` file from which the `DCV2T.orb` file is generated. The number of alpha electrons is the HOMO, the LUMO is HOMO+1

list:zindo\_orbitals

Listing 3.3: Gaussian input file `get_orbitals.com` used for generating molecular orbitals. The first line contains the name of the check file, the second the requested RAM. `int=zindos` requests the method ZINDO, `punch=mo` states that the molecular orbitals ought to be written to the `fort.7` file, `nosymm` forbids use of symmetry and is necessary to ensure correct position of orbitals with respect to the provided coordinates. The two integer numbers correspond to the charge and multiplicity of the system: 0 1 corresponds to a neutral system with a multiplicity of one. They are followed by the types and coordinates of all atoms in the molecule.

```
1090 %chk=DCV2T.chk
1091 %mem=100Mb
1092 #p int=zindos punch=mo nosymm
1093
1094 DCV2T molecular orbitals
1095
1096
1097 0 1
1098 S      -1.44650      2.12185      0.00135
1099 C      -2.43098      0.58936     -0.00048
1100 C      -1.59065     -0.51859     -0.00146
1101 C      -0.21222     -0.22233     -0.00095
1102 C       0.07761      1.13376      0.00040
1103 S       2.87651      0.79316      0.00148
1104 C       3.86099      2.32565      0.00235
1105 C       3.02066      3.43359      0.00231
1106 C       1.64223      3.13733      0.00162
1107 C       1.35240      1.78125      0.00114
1108 C      -3.85350      0.52245     -0.00081
1109 C      -4.79569      1.52479     -0.00008
1110 C      -6.18500      1.18622     -0.00117
1111 C      -4.47544      2.91565      0.00081
1112 C       5.28350      2.39256      0.00296
1113 C       6.22569      1.39020      0.00327
1114 C       7.61500      1.72876      0.00432
1115 C       5.90542     -0.00064      0.00333
1116 N      -7.32389      0.89743     -0.00195
1117 N      -4.21872      4.06274      0.00142
1118 N       8.75389      2.01754      0.00510
1119 N       5.64864     -1.14772      0.00361
1120 H      -1.98064     -1.52966     -0.00256
1121 H       0.55785     -0.98374     -0.00169
1122 H       3.41065      4.44466      0.00272
1123 H       0.87216      3.89874      0.00147
1124 H      -4.24640     -0.49192     -0.00188
1125 H       5.67641      3.40692      0.00337
```

## 3.4 Monomer calculations for DFT transfer integrals

list:edft\_gaussian\_xml

Listing 3.4: Example `package.xml` file for the Gaussian package required in the options of the `edft calculator` for the monomer calculations as preparation for the determination of transfer integrals using DIPRO.

```
1128 <package>
1129
```

```

1130 <name>gaussian</name>
1131 <executable>g09</executable>
1132 <checkpoint></checkpoint>
1133 <scratch></scratch>
1134
1135 <charge>0</charge>
1136 <spin>1</spin>
1137 <options># pop=minimal pbepbe/6-311g** scf=tight punch=mo nosymm test</options>
1138 <memory>1Gb</memory>
1139 <threads>2</threads>
1140
1141 <cleanup></cleanup>
1142 </package>

```

list:edft\_turbomole.xml

**Listing 3.5:** Example package.xml file for the Turbomole package required in the options of the edft calculator for the monomer calculations as preparation for the determination of transfer integrals using DIPRO.

```

1144 <package>
1145 <name>turbomole</name>
1146 <executable>ridft</executable>
1147 <scratch>/tmp</scratch>
1148
1149 <options>
1150 TITLE
1151 a coord
1152 *
1153 no
1154 b all def-TZVP
1155 *
1156 eht
1157 y
1158 0
1159 y
1160 dft
1161 on
1162 func
1163 pbe
1164 grid
1165 m3
1166 *
1167 ri
1168 on
1169 m 300
1170 *
1171 scf
1172 conv
1173 7
1174 iter
1175 200
1176 marij
1177
1178 q
1179
1180 </options>
1181
1182 <cleanup></cleanup>
1183 </package>

```

list:edft\_nwchem\_xml

Listing 3.6: Example `package.xml` file for the NWChem package required in the options of the `edft calculator` for the monomer calculations as preparation for the determination of transfer integrals using DIPRO.

```

1186 <package>
1187   <name>nwchem</name>
1188   <executable>nwchem</executable>
1189   <checkpoint></checkpoint>
1190   <scratch>/tmp/nwchem</scratch>
1191   <charge>0</charge>
1192   <spin>1</spin>
1193   <threads>1</threads>
1194   <memory></memory>
1195   <options>
1196     start
1197     basis
1198       * library 6-311gss
1199     end
1200     memory 1500 mb
1201   dft
1202     xc xpbe96 cpbe96
1203     direct
1204     iterations 100
1205     noprint "final vectors analysis"
1206   end
1207   task dft
1208 </options>
1209   <cleanup></cleanup>
1210 </package>
1211
1212
1213

```

## 3.5 Pair calculations for DFT transfer integrals

list:idft\_gaussian\_xml

Listing 3.7: Example `package.xml` file for the Gaussian package required in the options of the `idft calculator` for the pair calculations and the determination of transfer integrals using DIPRO.

```

1215 <package>
1216   <name>gaussian</name>
1217   <executable>g09</executable>
1218   <checkpoint></checkpoint>
1219   <scratch></scratch>
1220
1221   <charge>0</charge>
1222   <spin>1</spin>
1223   <options># pop=minimal pbepbe/6-311g** nosymm IOp(3/33=1,3/36=-1) punch=mo guess=cards scf=
1224   <memory>1Gb</memory>
1225   <threads>1</threads>
1226
1227   <cleanup></cleanup>
1228 </package>
1229
1230

```

list:idft\_turbomole\_xml

Listing 3.8: Example `package.xml` file for the Turbomole package required in the options of the `idft calculator` for the pair calculations and the determination of transfer integrals using DIPRO.

```

1231 <package>
1232   <name>turbomole</name>
1233

```

```

1234 <executable>ridft</executable>
1235 <scratch>/tmp</scratch>
1236
1237 <options>
1238 $intsdebug cao
1239 a coord
1240 *
1241 no
1242 b all def-TZVP
1243 *
1244 eht
1245 y
1246 0
1247 y
1248 dft
1249 on
1250 func
1251 pbe
1252 grid
1253 m3
1254 *
1255 ri
1256 on
1257 m 300
1258 *
1259 scf
1260 conv
1261 7
1262 iter
1263 1
1264 diis
1265 3
1266 damp
1267 0.00
1268
1269
1270
1271 marij
1272
1273 q
1274 </options>
1275
1276 <cleanup></cleanup>
1277 </package>
1278

```

list:ridft\_nwchem.xml

**Listing 3.9:** Example package.xml file for the NWChem package required in the options of the `idft` calculator for the pair calculations and the determination of transfer integrals using DIPRO.

```

1279
1280 <package>
1281 <name>nwchem</name>
1282 <executable>nwchem</executable>
1283 <checkpoint></checkpoint>
1284 <scratch>/tmp/nwchem</scratch>
1285 <charge>0</charge>
1286 <spin>1</spin>
1287 <memory></memory>
1288 <threads>1</threads>
1289 <options>
1290 start

```

```

1291 basis
1292   * library 6-311gss
1293 end
1294 memory 1500 mb
1295
1296 dft
1297   print "ao overlap"
1298   xc xpbe96 cpbe96
1299   direct
1300   iterations 1
1301   convergence nodamping nodiis
1302   noprint "final vectors analysis"
1303   vectors input system.movescs
1304 end
1305 task dft
1306 </options>
1307   <cleanup></cleanup>
1308 </package>

```

## 3.6 DFT transfer integrals

list:TI.xml

Listing 3.10: Example TI.xml file created as the output of a DIPRO calculation. Due to slightly different implementations, the orbitals indices refer to monomer indices in a Gaussian run but to indices in the merged dimer guess in a Turbomole run.

```

1311 <pair name="pair_100_155">
1312   <parameters>
1313     <HOMO_A>162</HOMO_A>
1314     <NoccA>1</NoccA>
1315     <LUMO_A>164</LUMO_A>
1316     <NvirtA>1</NvirtA>
1317     <HOMO_B>161</HOMO_B>
1318     <NoccB>1</NoccB>
1319     <LUMO_B>163</LUMO_B>
1320     <NvirtB>1</NvirtB>
1321   </parameters>
1322   <transport name="hole">
1323     <channel name="single">
1324       <J>1.546400416750696E-003</J>
1325       <e_A>-6.30726450715697</e_A>
1326       <e_B>-6.36775613794166</e_B>
1327     </channel>
1328     <channel name="multi">
1329       <molecule name="A">
1330         <e_HOMOm0>-6.30726450715697</e_HOMOm0>
1331       </molecule>
1332       <molecule name="B">
1333         <e_HOMOm0>-6.36775613794166</e_HOMOm0>
1334       </molecule>
1335       <dimer name="integrals">
1336         <T_00>1.546400416750696E-003</T_00>
1337         <J_sq_degen>2.391354248926727E-006</J_sq_degen>
1338         <J_sq_boltz>2.391354248926727E-006</J_sq_boltz>
1339       </dimer>
1340     </channel>
1341   </transport>
1342   <transport name="electron">

```

```

1344     <channel name="single">
1345         <J>-2.797473760331286E-003</J>
1346         <e_A>-4.50318366770689</e_A>
1347         <e_B>-4.53143397059021</e_B>
1348     </channel>
1349     <channel name="multi">
1350         <molecule name="A">
1351             <e_LUMOp0>-4.50318366770689</e_LUMOp0>
1352         </molecule>
1353         <molecule name="B">
1354             <e_LUMOp0>-4.53143397059021</e_LUMOp0>
1355         </molecule>
1356         <dimer name="integrals">
1357             <T_00>-2.797473760331286E-003</T_00>
1358             <J_sq_degen>7.825859439742066E-006</J_sq_degen>
1359             <J_sq_boltz>7.825859439742066E-006</J_sq_boltz>
1360         </dimer>
1361     </channel>
1362 </transport>
1363 </pair>

```

### 3.7 State file

1365

sec.statefile

1366 All data structures are saved to the `state.sql` file in sqlite3 format, see <http://www.sqlite.org/>.  
1367 They are available in form of tables in the `state.sql` file as can be seen by the command  
1368 `sqlite3 state.sql ".tables "`  
1369 An example of such a table are molecules. The full table can be displayed using the command  
1370 (similar for the other tables)  
1371 `sqlite3 state.sql "SELECT * FROM molecules "`  
1372 The meaning of all the entries in the table can be displayed by a command like  
1373 `sqlite3 state.sql ".SCHEMA molecules "`  
1374 The first and second entry are integers for internal and regular id of the molecule and the third  
1375 entry is the name. A single field from the table like the name of the molecule can be displayed by  
1376 a command like  
1377 `sqlite3 state.sql "SELECT name FROM molecules "`  
1378 Besides molecules, the following tables are stored in the `state.sql`:  
1379 `conjseg_properties`:  
1380 Conjugated segments are stored with id, name and x,y,z coordinates of the center of mass in nm.  
1381 `conjsegs`:  
1382 Reorganization energies for charging or discharging a conjugated segment are stored together  
1383 with the coulomb energy and any other user defined energy contribution (in eV) and occupation  
1384 probabilities.  
1385 `pairs`:  
1386 The pairs from the neighborlist are stored with the pair id, the id of the first and second segment,  
1387 the rate from the first to the second , the rate from the second to the first (both in s<sup>-1</sup>) and the  
1388 x,y,z coordinates in nm of the distance between the first and the second segment.  
1389 `pairintegrals`:  
1390 Transfer integrals for all pairs are stored in the following way: The pair id , the number for count-  
1391 ing possible different electronic overlaps (e.g if only the frontier orbitals are taken into account  
1392 this is always zero, while an effective value is stored in addition to the different overlaps of e.g.  
1393 HOMO-1 and HOMO-1 if more frontier orbitals are taken into account) and the integral in eV.  
1394 `pairproperties`:  
1395 The outer sphere reorganization energy of all pairs is stored by an id, the pair id, a string `lambda_outer`  
1396 and the energy in eV.

```

1397 conjsegs:
1398 Conjugated segments are saved in the following way: The id, the name, the type, the molecule
1399 id, the time frame, the x,y,z coordinates in nm and the occupation probability.
1400 conjseg_properties:
1401 Properties of the conjugated segments like reorganization energies for charging or discharging a
1402 charge unit or the coulomb contribution to the site energy are stored by: id, conjugated segment
1403 id, a string like lambda_intra_charging, lambda_intra_discharging or energy_coulomb
1404 and a corresponding value in eV.
1405 The tables rigidfrag_properties, rigidfrags and frames offer information about rigid
1406 fragments and time frames including periodic boundary conditions.
1407 The data in the state.sql file can also be modified by the user. Here is an example how to
1408 modify the transfer integral between the conjugated segments number one and two assuming
1409 that they are in the neighborlist. Their pair id can be found by the command
1410 pair_ID='sqlite3 state.sql "SELECT _id FROM pairs WHERE conjseg1=1 AND conjseg2=2"'
1411 The old value of the transfer integral can be deleted using
1412 sqlite3 state.sql "DELETE FROM pair_integrals WHERE pair=$pair_ID"
1413 Finally the new transfer integral  $J$  can be written to the state.sql file by the command
1414 sqlite3 state.sql "INSERT INTO pair_integrals (pair,num,J) VALUES ($pair_ID,0,$J) "
1415 Here the num=0 indicates that only the effective transfer integrals is written to the file, while other
1416 values of num would correspond to overlap between other orbitals than the frontier orbitals.
1417 In a similar way the coulomb contribution to the site energy of the first conjugated segment can
1418 be overwritten by first getting its id
1419 c_ID='sqlite3 state.sql "SELECT _id from conjseg_properties where conjseg=1 AND
1420 key =\"energy_coulomb\""
1421 Then deleting the old value
1422 sqlite3 state.sql "DELETE FROM conjseg_properties WHERE _id=$c_ID"
1423 Then the new coulomb energy  $E$  can be written to this id
1424 sqlite3 state.sql "INSERT INTO conjseg_properties (_id,conjseg,key,value)
1425 VALUES ($c_ID,1,\"energy_coulomb\",$E) "
1426 Finally the resulting coulomb contribution to all conjugated segments can be displayed by
1427 sqlite3 state.sql "SELECT * from conjseg_properties WHERE key=\"energy_coulomb\""
1428

```





## 1429 Chapter 4

## 1430 Reference

sec:reference

### 1431 4.1 Programs

sec:programs

1432 Programs execute specific tasks (calculators).

#### 1433 4.1.1 xtp\_map

prog:xtp\_map

1434 Generates QM|MD topology

1435     -h [ --help ] display this help and exit  
1436     -v [ --verbose ] be loud and noisy  
1437     -t [ --topology ] arg topology  
1438     -c [ --coordinates ] arg coordinates or trajectory  
1439     -s [ --segments ] arg definition of segments and fragments  
1440     -f [ --file ] arg state file

#### 1441 4.1.2 xtp\_run

prog:xtp\_run

1442 Runs excitation/charge transport calculators

1443     -h [ --help ] display this help and exit  
1444     -v [ --verbose ] be loud and noisy  
1445     -o [ --options ] arg calculator options  
1446     -f [ --file ] arg sqlight state file, \*.sql  
1447     -i [ --first-frame ] arg (=1) start from this frame  
1448     -n [ --nframes ] arg (=1) number of frames to process  
1449     -t [ --nthreads ] arg (=1) number of threads to create  
1450     -s [ --save ] arg (=1) whether or not to save changes to state file  
1451     -e [ --execute ] arg List of calculators separated by ',' or ''  
1452     -l [ --list ] Lists all available calculators  
1453     -d [ --description ] arg Short description of a calculator

#### 1454 4.1.3 xtp\_tools

prog:xtp\_tools

1455 Runs excitation/charge transport tools

1456     -h [ --help ] display this help and exit  
1457     -v [ --verbose ] be loud and noisy  
1458     -o [ --options ] arg calculator options  
1459     -t [ --nthreads ] arg (=1) number of threads to create Tools:  
1460     -e [ --execute ] arg List of tools separated by ',' or ''  
1461     -l [ --list ] Lists all available tools

```
1462     -d [ --description ] arg Short description of a tool
```

#### 1463 4.1.4 xtp\_parallel

prog:xtp\_parallel

```
1464 Runs job-based heavy-duty calculators
```

```
1465     -h [ --help ] display this help and exit
1466     -v [ --verbose ] be loud and noisy
1467     -o [ --options ] arg calculator options
1468     -f [ --file ] arg sqlite state file, *.sql
1469     -i [ --first-frame ] arg (=1) start from this frame
1470     -n [ --nframes ] arg (=1) number of frames to process
1471     -t [ --nthreads ] arg (=1) number of threads to create
1472     -s [ --save ] arg (=1) whether or not to save changes to state file
1473     -r [ --restart ] arg restart pattern: 'host(pc1:234) stat(FAILED)'
1474     -c [ --cache ] arg (=8) assigns jobs in blocks of this size
1475     -j [ --jobs ] arg (=run) task(s) to perform: input, run, import
1476     -m [ --maxjobs ] arg (=1) maximum number of jobs to process (-1 = inf)
1477     -e [ --execute ] arg List of calculators separated by ',' or ''
1478     -l [ --list ] Lists all available calculators
1479     -d [ --description ] arg Short description of a calculator
```

#### 1480 4.1.5 xtp\_dump

prog:xtp\_dump

```
1481 Extracts information from the state file
```

```
1482     -h [ --help ] display this help and exit
1483     -v [ --verbose ] be loud and noisy
1484     -o [ --options ] arg calculator options
1485     -f [ --file ] arg sqlight state file, *.sql
1486     -i [ --first-frame ] arg (=1) start from this frame
1487     -n [ --nframes ] arg (=1) number of frames to process
1488     -t [ --nthreads ] arg (=1) number of threads to create
1489     -s [ --save ] arg (=1) whether or not to save changes to state file Extractors:
1490     -e [ --extract ] arg List of extractors separated by ',' or ''
1491     -l [ --list ] Lists all available extractors
1492     -d [ --description ] arg Short description of an extractor
```

#### 1493 4.1.6 xtp\_update\_exciton

prog:xtp\_update\_exciton

```
1494 Updates the CTP state file to additionally use singlets and triplets + optional arguments:
```

```
1495     -h, --help show this help message and exit
1496     -f SQLFILE, --file SQLFILE State file to update.
```

#### 1497 4.1.7 xtp\_basisset

prog:xtp\_basisset

```
1498 xtp_update, version 1.6-dev gitid: f7e5739 Creates votca xml basissetfiles from NWChem basis-
1499 setfiles optional arguments:
```

```
1500     -h, --help show this help message and exit
1501     -f INPUT, --input INPUT NWchem file containing the basisset or Turbomole folder
1502     with element names.
1503     -o OUTPUTFILE, --outputvotca OUTPUTFILE Path of votca outputfile
1504     -t TURBOBASIS, --turbomolebasisset TURBOBASIS For turbomole specify the ba-
1505     sisset that is supposed to be extracted from Files, for auxbasis sets the basisset the aux ba-
1506     sisset is supposed to be used for.
```

### 4.1.8 xtp\_makeauxbasis

xtp\_update, version 1.6-dev gitid: f7e5739 Creates votca xml aux-basissetfiles from votca basis-setfiles optional arguments:

```
-h, --help show this help message and exit
-f BASISFILE, --basisfile BASISFILE xtp basissetfile
-o OUTFILE, --outfile OUTFILE optional file to write basisset to
-g GROUPING, --grouping GROUPING Cutoff at which basisfunctions are grouped together in deviation from the arithmetic mean; Default 0.1
-c CUTOFF, --cutoff CUTOFF Cutoff for very localised basisfunctions; Default 60
-e ELEMENT, --element ELEMENT Print out only the element specified
-l LMAX, --lmax LMAX maximum angular momentum in aux basisset: Default:4
```

## 4.2 Calculators

Calculator is a piece of code which computes specific system properties, such as site energies, transfer integrals, etc. `xtp_run`, `xtp_kmc_run` are wrapper programs which executes such calculators. The generic syntax is

```
xtp_run -e "calc1, calc2, ..." -o options.xml
```

File `options.xml` lists all options needed to run a specific calculator. The format of this file is explained in listing 4.1. A complete list of calculators is given in the [calculators](#) reference section.

Listing 4.1: A part of the `options.xml` file with options for the `calculator_name{1,2}` [calculators](#).

```
<calculator_name1>
  <option1>value1</option1>
  <option2>value2</option2>
  ...
</calculator_name1>
<calculator_name2>
  <option1>value1</option1>
  <option2>value2</option2>
  ...
</calculator_name2>
...
```

A list of all calculators and their short descriptions can be obtain using

```
xtp_run --list
```

A detailed description of all options of a specific calculator(s) is available via

```
xtp_run --desc calc1,calc2,...
```

## 4.3 Common options

name	Description of the option
------	---------------------------



# Bibliography

- ruhle\_microscopic\_2011 [1] V. Rühle *et al.*, J. Chem. Theory Comput. **7**, 3335 (2011), bibtex: ruhle\_microscopic\_2011.
- ruhle\_versatile\_2009 [2] V. Rühle *et al.*, Journal of Chemical Theory and Computation **5**, 3211 (2009), bibtex: ruhle\_versatile\_2009.
- gamma\_design\_1995 [3] E. Gamma, R. Helm, and R. E. Johnson, *Design Patterns. Elements of Reusable Object-Oriented Software.*, 1st ed., reprint. ed. (Addison-Wesley Longman, Amsterdam, ADDRESS, 1995), bibtex: gamma\_design\_1995.
- ruhle\_multiscale\_2010 [4] V. Rühle, J. Kirkpatrick, and D. Andrienko, The Journal of Chemical Physics **132**, 134103 (2010), bibtex: ruhle\_multiscale\_2010.
- vukmirovic\_charge\_2008 [5] N. Vukmirović and L.-W. Wang, The Journal of Chemical Physics **128**, 121102 (2008), bibtex: vukmirovic\_charge\_2008.
- vukmirovic\_charge\_2009 [6] N. Vukmirović and L.-W. Wang, Nano Letters **9**, 3996 (2009), bibtex: vukmirovic\_charge\_2009.
- mcmahon\_ad\_2009 [7] D. P. McMahon and A. Troisi, Chemical Physics Letters **480**, 210 (2009), bibtex: mcmahon\_ad\_2009.
- bredas\_charge-transfer\_2004 [8] J.-L. Brédas, D. Beljonne, V. Coropceanu, and J. Cornil, Chemical Reviews **104**, 4971 (2004), bibtex: bredas\_charge-transfer\_2004.
- may\_relationship\_2011 [9] F. May *et al.*, Journal of Materials Chemistry **21**, 9538 (2011), bibtex: may\_relationship\_2011.
- breneman\_determining\_1990 [10] C. M. Breneman and K. B. Wiberg, Journal of Computational Chemistry **11**, 361 (1990), bibtex: breneman\_determining\_1990.
- stone\_distributed\_1985 [11] A. Stone and M. Alderton, Molecular Physics **56**, 1047 (1985), bibtex: stone\_distributed\_1985.
- chirlian\_atomic\_1987 [12] L. E. Chirlian and M. M. Francl, Journal of Computational Chemistry **8**, 894 (1987), bibtex: chirlian\_atomic\_1987.
- singh\_approach\_1984 [13] U. C. Singh and P. A. Kollman, Journal of Computational Chemistry **5**, 129 (1984), bibtex: singh\_approach\_1984.
- stone\_distributed\_2005 [14] A. J. Stone, J. Chem. Theory Comput. **1**, 1128 (2005), bibtex: stone\_distributed\_2005.
- stone\_theory\_1997 [15] A. J. Stone, *The Theory of intermolecular forces* (Clarendon Press, Oxford, 1997), bibtex: stone\_theory\_1997.
- thole\_molecular\_1981 [16] B. Thole, Chemical Physics **59**, 341 (1981), bibtex: thole\_molecular\_1981.
- van\_duijnen\_molecular\_1998 [17] P. T. van Duijnen and M. Swart, The Journal of Physical Chemistry A **102**, 2399 (1998), bibtex: van\_duijnen\_molecular\_1998-1.
- applequist\_atom\_1972 [18] J. Applequist, J. R. Carl, and K.-K. Fung, Journal of the American Chemical Society **94**, 2952 (1972), bibtex: applequist\_atom\_1972.
- ren\_polarizable\_2003 [19] P. Ren and J. W. Ponder, The Journal of Physical Chemistry B **107**, 5933 (2003), bibtex: ren\_polarizable\_2003.
- baessler\_charge\_1993 [20] H. Baessler, Physica Status Solidi B **175**, 15 (1993), bibtex: baessler\_charge\_1993.
- troisi\_charge-transport\_2006 [21] A. Troisi and G. Orlandi, Phys. Rev. Lett. **96**, (2006), bibtex: troisi\_charge-transport\_2006.
- troisi\_charge\_2009 [22] A. Troisi, D. L. Cheung, and D. Andrienko, Physical Review Letters **102**, 116602 (2009), bibtex: troisi\_charge\_2009.
- mcmahon\_organic\_2010 [23] D. P. McMahon and A. Troisi, ChemPhysChem **11**, 2067 (2010), bibtex: mcmahon\_organic\_2010.
- vehoff\_charge\_2010 [24] T. Vehoff *et al.*, The Journal of Physical Chemistry C **114**, 10592 (2010), bibtex: vehoff\_charge\_2010.
- baumeier\_density-functional\_2010 [25] B. Baumeier, J. Kirkpatrick, and D. Andrienko, Physical Chemistry Chemical Physics **12**, 11103 (2010), bibtex: baumeier\_density-functional\_2010.

- kirkpatrick\_approximate\_2008 [26] J. Kirkpatrick, International Journal of Quantum Chemistry **108**, 51 (2008), bibtex: kirkpatrick\_approximate\_2008.
- walker\_electrical\_2002 [27] A. B. Walker, A. Kambili, and S. J. Martin, Journal of Physics: Condensed Matter **14**, 9825 (2002), bibtex: walker\_electrical\_2002.
- borsenberger\_charge\_1991 [28] P. M. Borsenberger, L. Pautmeier, and H. Bässler, The Journal of Chemical Physics **94**, 5447 (1991), bibtex: borsenberger\_charge\_1991.
- pasveer\_unified\_2005 [29] W. F. Pasveer *et al.*, Physical Review Letters **94**, 206601 (2005), bibtex: pasveer\_unified\_2005.
- bredas\_molecular\_2009 [30] J.-L. Brédas, J. E. Norton, J. Cornil, and V. Coropceanu, Accounts of Chemical Research **42**, 1691 (2009), bibtex: bredas\_molecular\_2009.
- coropceanu\_charge\_2007 [31] V. Coropceanu *et al.*, Chemical Reviews **107**, 926 (2007), bibtex: coropceanu\_charge\_2007.
- nelson\_modeling\_2009 [32] J. Nelson, J. J. Kwiatkowski, J. Kirkpatrick, and J. M. Frost, Accounts of Chemical Research **42**, 1768 (2009), bibtex: nelson\_modeling\_2009.
- marcus\_electron\_1993 [33] R. A. Marcus, Reviews of Modern Physics **65**, 599 (1993), bibtex: marcus\_electron\_1993.
- hutchison\_hopping\_2005 [34] G. R. Hutchison, M. A. Ratner, and T. J. Marks, Journal of the American Chemical Society **127**, 2339 (2005), bibtex: hutchison\_hopping\_2005.
- chang\_new\_2005 [35] J.-L. Chang, Journal of Molecular Spectroscopy **232**, 102 (2005), bibtex: chang\_new\_2005.
- hoffman\_reorganization\_1996 [36] B. M. Hoffman and M. A. Ratner, Inorganica Chimica Acta **243**, 233 (1996), bibtex: hoffman\_reorganization\_1996.
- bortz\_new\_1975 [37] A. B. Bortz, M. H. Kalos, and J. L. Lebowitz, Journal of Computational Physics **17**, 10 (1975), bibtex: bortz\_new\_1975.
- scher\_anomalous\_1975 [38] H. Scher and E. Montroll, Physical Review B **12**, 2455 (1975), bibtex: scher\_anomalous\_1975.
- borsenberger\_role\_1993 [39] P. M. Borsenberger, E. H. Magin, M. D. VanAuweraer, and F. C. D. Schryver, Physica Status Solidi A **140**, 9 (1993), bibtex: borsenberger\_role\_1993.
- derrida\_velocity\_1983 [40] B. Derrida, Journal of Statistical Physics **31**, 433 (1983), bibtex: derrida\_velocity\_1983.
- cordes\_one-dimensional\_2001 [41] H. Cordes *et al.*, Physical Review B **63**, 094201 (2001), bibtex: cordes\_one-dimensional\_2001.
- seki\_electric\_2001 [42] K. Seki and M. Tachiya, Physical Review B **65**, 014305 (2001), bibtex: seki\_electric\_2001.
- lukyanov\_extracting\_2010 [43] A. Lukyanov and D. Andrienko, Physical Review B **82**, 193202 (2010), bibtex: lukyanov\_extracting\_2010.
- van\_der\_holst\_modeling\_2009 [44] J. J. M. van der Holst *et al.*, Physical Review B **79**, 085203 (2009), bibtex: van\_der\_holst\_modeling\_2009.
- dunlap\_charge-dipole\_1996 [45] D. Dunlap, P. Parris, and V. Kenkre, Physical Review Letters **77**, 542 (1996), bibtex: dunlap\_charge-dipole\_1996.
- novikov\_essential\_1998 [46] S. V. Novikov *et al.*, Physical Review Letters **81**, 4472 (1998), bibtex: novikov\_essential\_1998.
- nagata\_atomistic\_2008 [47] Y. Nagata and C. Lennartz, The Journal of Chemical Physics **129**, 034709 (2008), bibtex: nagata\_atomistic\_2008.
- novikov\_cluster\_1995 [48] S. V. Novikov and A. V. Vannikov, The Journal of Physical Chemistry **99**, 14573 (1995), bibtex: novikov\_cluster\_1995.